iScience

CellPress
OPEN ACCESS

Article

Impact of mutations defining SARS-CoV-2 Omicron subvariants BA.2.12.1 and BA.4/5 on Spike function and neutralization

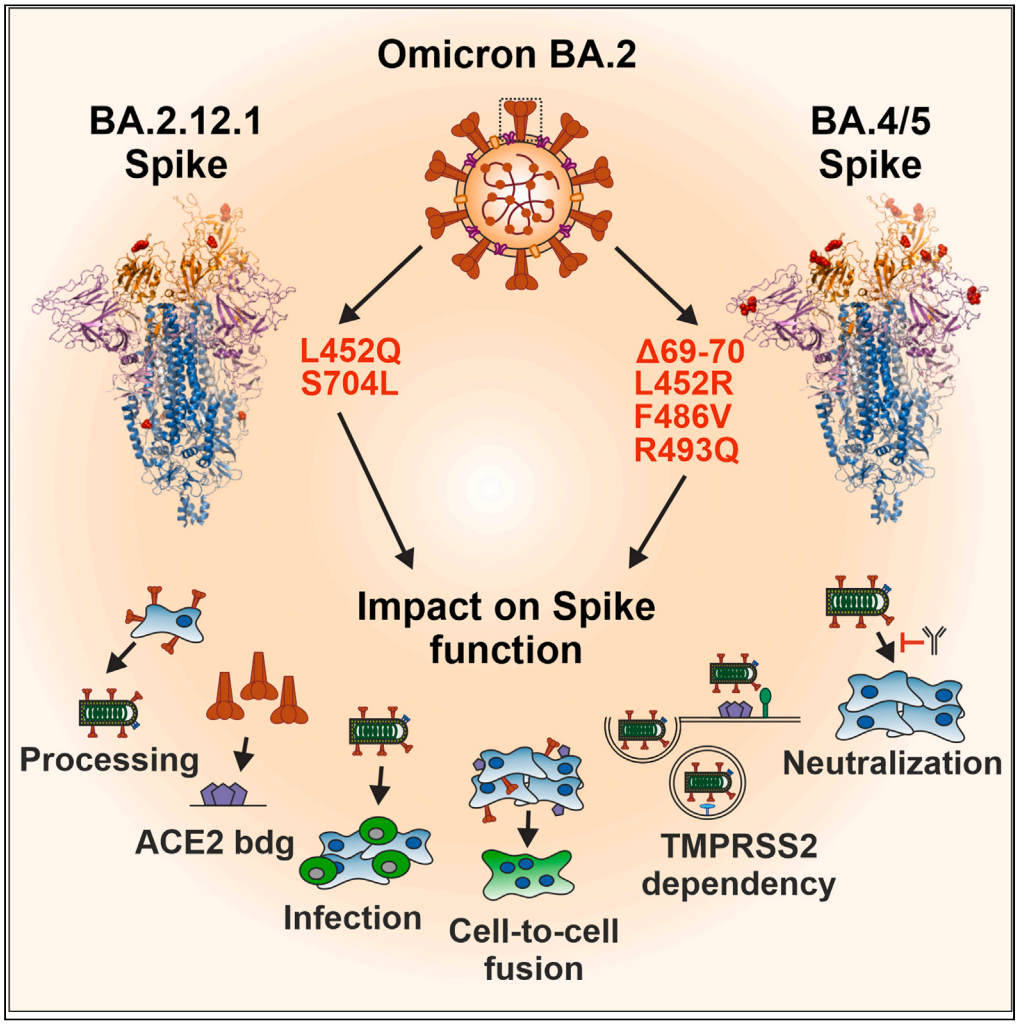

Chiara Pastorio, Sabrina Noettger, Rayhane Nchioua, Fabian Zech, Konstantin M.J. Sparrer, Frank Kirchhoff

Frank.Kirchhoff@uni-ulm.de

Highlights

Spike activity of Omicron subvariants is increasing (BA.1<BA.2<BA.2.12.1< BA.4/5)

L452Q/R and F486V enhance and R493Q or S704L reduce BA.2 Spike-mediated infection

Δ69-70, L452R, and F486V contribute to increased fusogenicity of BA.4/5 Spike

Combined mutations are required for full activity of BA.4/5 Spike

Pastorio et al., iScience 26, 108299
November 17, 2023
https://doi.org/10.1016/j.isci.2023.108299

iScience

CellPress
OPEN ACCESS

Article

Impact of mutations defining SARS-CoV-2 Omicron subvariants BA.2.12.1 and BA.4/5 on Spike function and neutralization

Chiara Pastorio,[1] Sabrina Noettger,[1] Rayhane Nchioua,[1] Fabian Zech,[1] Konstantin M.J. Sparrer,[1] and Frank Kirchhoff[1,2,*]

SUMMARY

Additional mutations in the viral Spike protein helped the BA.2.12.1 and BA.4/5 SARS-CoV-2 Omicron subvariants to outcompete the parental BA.2 subvariant. Here, we determined the functional impact of mutations that newly emerged in the BA.2.12.1 (L452Q, S704L) and BA.4/5 (Δ69-70, L452R, F486V, R493Q) Spike proteins. Our results show that mutation of L452Q/R or F486V typically increases and R493Q or S704L impair BA.2 Spike-mediated infection. In combination, changes of Δ69-70, L452R, and F486V contribute to the higher infectiousness and fusogenicity of the BA.4/5 Spike. L452R/Q and F486V in Spike are mainly responsible for reduced sensitivity to neutralizing antibodies. However, the combined mutations are required for full infectivity, reduced TMPRSS2 dependency, and immune escape of BA.4/5 Spike. Thus, it is the specific combination of mutations in BA.4/5 Spike that allows increased functionality and immune evasion, which helps to explain the temporary dominance and increased pathogenicity of these Omicron subvariants.

INTRODUCTION

The coronavirus polymerase has proof-reading activity and consequently, *Coronaviridae* are much less variable than other RNA viruses, such as HIV or HCV.[1,2] Nonetheless, the enormous spread of SARS-CoV-2, with more than 700 million infections in the past three years, allowed this virus to evolve numerous adaptations promoting efficient transmission and immune evasion in the new human host.[3,4] The most successful SARS-CoV-2 variants were called variants of concern (VOCs) and specified by Greek letters. The five current VOCs (Alpha, Beta, Gamma, Delta, and Omicron) all evolved independently from early SARS-CoV-2 strains and sequentially replaced one another.[5] This changed with the emergence of Omicron that outcompeted the Delta VOC and dominates the COVID-19 pandemic since the end of 2021.[4] Alterations in the viral Spike (S) protein play a key role in the emergence of novel Omicron subvariants. The main function of SARS-CoV-2 S is to mediate entry into target cells via the cellular angiotensin-converting enzyme 2 (ACE2) receptor.[6,7] In addition, S is the main target of neutralizing antibodies. The initial Omicron BA.1 variant differs by ~35 mutations in its S protein from previous SARS-CoV-2 strains and shows substantially reduced susceptibility to neutralizing antibodies induced by previous COVID-19 infection or vaccination.[8–10] However, BA.1 was reported to be less infectious and pathogenic than the Delta SARS-CoV-2 VOC.[11,12] It was rapidly replaced by BA.2, which shares ~20 mutations in S with BA.1 but also contains ~10 strain-specific alterations.[13]

All SARS-CoV-2 variants that dominate the COVID-19 pandemic since the middle of 2022 evolved from the BA.2 VOC.[3] The structural and functional properties of S proteins from the different SARS-CoV-2 VOCs including BA.1 and BA.2, as well as their susceptibility to neutralization by sera from vaccinated individuals or therapeutic antibodies have been addressed in previous studies.[13–15] Altogether, the results showed that numerous alterations in the N-terminal domain (NTD) and/or receptor binding domain (RBD) of BA.1 and/or BA.2 S proteins cooperate to promote efficient viral humoral immune evasion.[13,16] In addition, it has been reported that the BA.1 VOC is less active than earlier SARS-CoV-2 variants in many cell culture systems as well as animal models and that BA.2 gained increased replication fitness.[11,17,18]

In part, the original BA.2 VOC was temporarily displaced by the BA.2.12.1 subvariant before both were outcompeted by BA.4/5 in the second half of 2022.[19,20] BA.2.12.1 S differs only by two mutations (L452Q and S704L) from its BA.2 precursor.[21] BA.4 and BA.5 have identical S amino acid sequences but contain variations in the NSP1, ORF7b, and N proteins.[5,22] Compared to BA.2, the BA.4/5 S contains three characteristic mutations (Δ69-70, L452R, and F486V) and a reversion to early SARS-CoV-2 strains (R493Q).[19] It has been established that BA.4/5 S is more fusogenic than BA.2 S and resistant to most neutralizing antibodies[18,23–25] but the functional impact of individual amino acid changes that are characteristic for BA.4/5 S proteins is incompletely understood. Expanding our previous analyses of mutations found in BA.1 and BA.2 S proteins,[13] we thus introduced BA.2.12.1 and BA.4/5 defining mutations and combinations thereof in the parental BA.2 S and

[1]Institute of Molecular Virology, Ulm University Medical Centre, 89081 Ulm, Germany
[2]Lead contact
*Correspondence: Frank.Kirchhoff@uni-ulm.de
https://doi.org/10.1016/j.isci.2023.108299

determined their impact on viral pseudo-particle infectivity, cell-to-cell fusion, dependency on TMPRSS2 and cathepsins, as well as susceptibility to therapeutic agents and neutralization. Our results reveal that specific combinations of amino acid changes are required for the enhanced fusogenicity, infectiousness, and full humoral immune evasion capacity of the BA.4/5 S protein.

RESULTS

Generation of S proteins containing BA.2.12.1 and BA.4/5 defining mutations

Omicron has diversified into various sublineages that emerged from BA.2, such as BA.2.12.1, BA.4/5 (containing identical S sequences), BQ1.1, and XBB1.5 (Figure 1A).[26] BA.4 and subsequently BA.5 have replaced BA.2 and dominated the COVID-19 pandemic from mid to end of 2022, while BA.2.12.1 was temporarily responsible for up to 20% of all infections worldwide in mid of 2022 (Figure 1B). Three of the four BA.4/5 defining mutations were also present in earlier SARS-CoV-2 variants (e.g., Δ69-70 in Alpha and BA.1, L452R in Delta and R493Q in most early strains). Thus, their frequency fluctuated over time (Figure 1B). Four of the six mutations that distinguish BA.2.12.1 (L452Q) or BA.4/5 (L452R, F486V, and R493Q) S proteins from BA.2 are located in the RBD that interacts with ACE2 (Figure 1C). The two remaining changes are located in the NTD (Δ69-70) of BA.4/5 S and in the region between the S1/S2 and S2′ cleavage sites (S704L) in BA.2.12.1 S (Figure 1D). To examine their functional impact, the six mutations found in BA.2.12.1 or BA.4/5 S were introduced individually and in combination in the parental BA.2 S protein. To assess potential dependencies on the S backbone, we also introduced changes of L452Q/R, F486V, and S704L into the S protein of the early Hu-1 SARS-CoV-2 strain, which differs from BA.2 by a total of 28 point mutations and one deletion (Figure 1D). Sequence analyses verified that only the desired mutations were present in the set of 21 mutant S expression constructs generated.

Impact of BA.2.12.1 and BA.4/5 defining mutations on Spike expression and processing

To examine the functional impact of mutations characterizing BA.2.12.1 and BA.4/5 S proteins, we used pseudotyped vesicular stomatitis virus (VSVpp) particles recapitulating key features of SARS-CoV-2 infection, including receptor usage, cell tropism, protease dependency, and susceptibility to neutralizing antibodies.[6,27,28] Western blot analyses of HEK293T cells transfected with S expression constructs and transduced with VSVΔG-eGFP and the S-containing VSVpp in the culture supernatants showed that all S protein variants were efficiently expressed, processed, and incorporated into VSVpp (Figure S1A). BA.2-based S proteins were generally processed with lower efficiency than Hu-1-based S proteins but the differences failed to reach significance (Figure S1B, lower panel). However, similar levels and ratios of Hu-1, BA.2, BA.2.12.1, and BA.4/5 full-length S and processed S2 proteins were detected in VSVpp (Figure S1B, upper panel). Mutations of F486V, R493Q, and S704L in BA.2 S moderately reduced the levels of S2 in VSVpp. Unlike a previous report,[29] we did not observe an enhancing effect of L452R on proteolytic S processing. To identify potential differences in ACE2 interaction, we incubated immobilized ACE2 with lysates of HEK293T cells transfected with S expression constructs and determined how much S protein is retained after washing, as previously reported.[30] In agreement with the previous finding that BA.2.12.1 and BA.4/5 S proteins bind ACE2 efficiently and with similar affinity as previous VOCs,[18,21,31] all parental and mutant S proteins showed efficient ACE2 binding (Figure S1C). Reversion of R493Q either individually or in combination with the Δ69-70, L452R, and/or F486V changes slightly reduced the levels of BA.2-based S proteins bound to ACE2. Notably, the impact of the individual R493Q change was not significant (Figure S1C), and previous studies suggested that the R493Q mutation in S promotes ACE2 interaction.[21,32] Our approach does not allow to quantify binding affinities and is thus not contradictory to the previous reports. Altogether, our results showed efficient expression, processing, and ACE2 binding of all S proteins analyzed.

Impact of BA.4/5 defining mutations on S-mediated infection

To understand which mutations in BA.4/5 promote particle entry, we examined S-mediated VSVpp infection in the intestinal epithelial cell line Caco2 and alveolar A549 cells engineered to stably express ACE2 alone or together with TMPRSS2. We used three different cell lines to assess the robustness of the effects in both intestinal (Caco2) and pulmonary (A549) cells. In addition, Caco2 cells are useful because they allow S-mediated VSVpp infection at endogenous levels of ACE2 expression and since the gut is a relevant target for SARS-CoV-2 infection.[33,34] We also used A549 cells because they are derived from the lung (the primary viral target) and allowed to examine the impact of TMPRSS2 overexpression on infection efficiencies mediated by mutant and parental Spike proteins.[35] To examine effects of the mutations on S function, we normalized the VSVpp stocks for the same levels of M protein. Automated quantification of VSVpp-infected GFP+ cells showed that Hu-1 S was most effective in mediating infection of Caco2 cells, while BA.4/5 S was most efficient in A549 cells (Figures 2A–2C and S2A). Overexpression of TMPRSS2 increased infection rates of A549 cells ~10-fold. Viral entry mediated by S proteins of Omicron subvariants gradually increased from BA.1, BA.2, BA.2.12.1 to BA.4/5 (Figure 2B), reflecting their order of emergence in the human population (Figure 1B). None of the individual mutations significantly affected Hu-1 S-mediated infection, except for a moderate increase by L452Q in A549-ACE2-TMPRSS2 cells (Figures 2C and S2A). However, individual mutations of S704L and (less severely) R493Q reduced infection in all three cell lines in the context of BA.2 S (Figures 2C and S2A).

To elucidate the causes for changes in VSVpp infection efficiencies, we quantified the levels of expression, processing, and virion incorporation of all mutant S proteins relative to the BA.2 S. Quantification of the signals obtained in western blot analyses (Figure S1A) showed that most mutations had little effect on S expression and processing in transfected HEK293T cells (Figure S2B). However, the levels of total S and (more strongly) processed S2 were increased for BA.4/5 and the Δ69-70 mutant compared to the BA.2 S protein. Altogether, the efficiency of VSVpp infection correlated with the levels of processed S2 protein in the culture supernatants (Figure S2B, upper panel). The

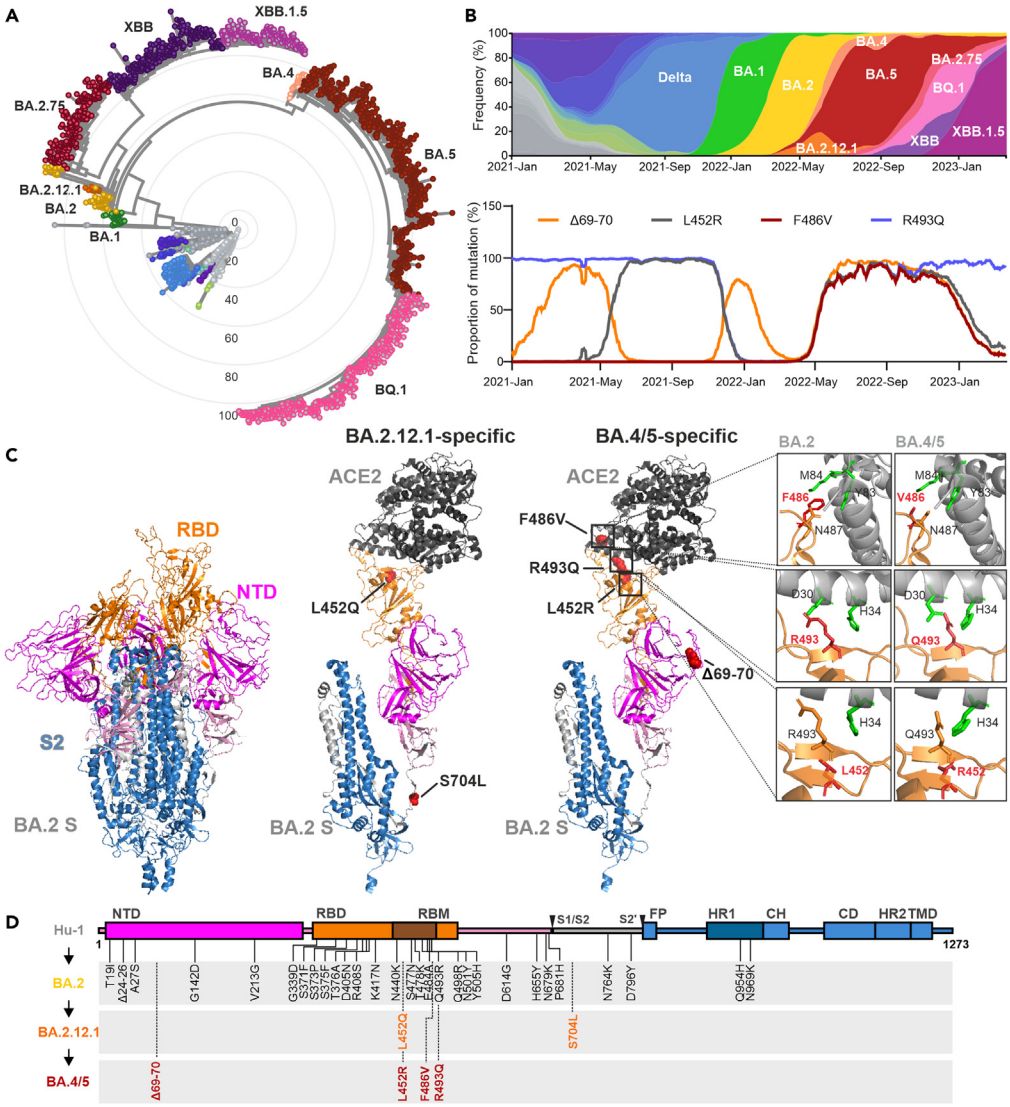

Figure 1. Features of Omicron BA.2.12.1 and BA.4/5 VOCs

(A) Radial phylogenetic tree of representative SARS-CoV-2 strains (n = 2,652 genomes, sampled between December 2019 and April 2023) scaled according to their divergence compared to the Hu-1 sequence. Retrieved from Nextstrain on April 5th 2023 (https://nextstrain.org/ncov/open/global/6m?l= radial&m=div) and modified. Color coding according to VOCs as indicated.

(B) The upper panel shows the frequencies of SARS-CoV-2 Delta and Omicron BA.1, BA.2, BA.2.12.1, BA.4, BA.5, BA.2.75, BQ.1, XBB, and XBB.1.5 sequences from January 2021 to April 2023. Scaled to 100%. Retrieved and modified from Nextstrain on April 5th 2023. The lower panel shows the proportion of sequences containing the indicated amino acid changes relative to the total number of sequences (100%) at the indicated time points, obtained from covSpectrum and modified (https://cov-spectrum.org/explore/World/AllSamples/AllTimes/variants).

(C) Overview on the SARS-CoV-2 BA.2 S structure (PDB: 7XIW) or of one BA.2 S monomer bound to human ACE2 (PDB: 7XO7) and localization of amino acid changes specific for BA.2.12.1 or BA.4/5 as indicated. The right panel provides a close-up view of differences between BA.2 (PDB: 7XO7) and BA.4/5 S (PDB: 7XWA) (right panel). NTD (lavander purple), RBD (orange), RBM (brown), S2 (blue), ACE2 (gray), and mutations (red).

(D) Schematic depiction of the SARS-CoV-2 S, its domains and amino acid alterations in Omicron BA.2 (black), BA.2.12.1 (orange), and BA.4/5 (dark red) VOCs compared to the Hu-1 sequence. S1 subunit: N-terminal domain, NTD (lavender purple), receptor binding domain, RBD (orange), and receptor binding motif, RBM (brown). S2 subunit: fusion peptide, FP (blue), heptad repeat 1, HR1 (dark blue) central helix, CH, connector domain, CD, heptad repeat 2, HR2, and transmembrane domain, TM (blue).

levels of BA.4/5 S2 protein were about 3-fold increased compared to BA.2 S2 suggesting that efficient processing and virion incorporation contributes to its high activity. In comparison, mutation of R493Q reduced S2 levels by ~10% and infection by ~30% (Figure S2B). Thus, other than previously suggested,[21,32] this change reduced rather than increased S-mediated infection (Figures S1A, S1B, and S2B). However, the

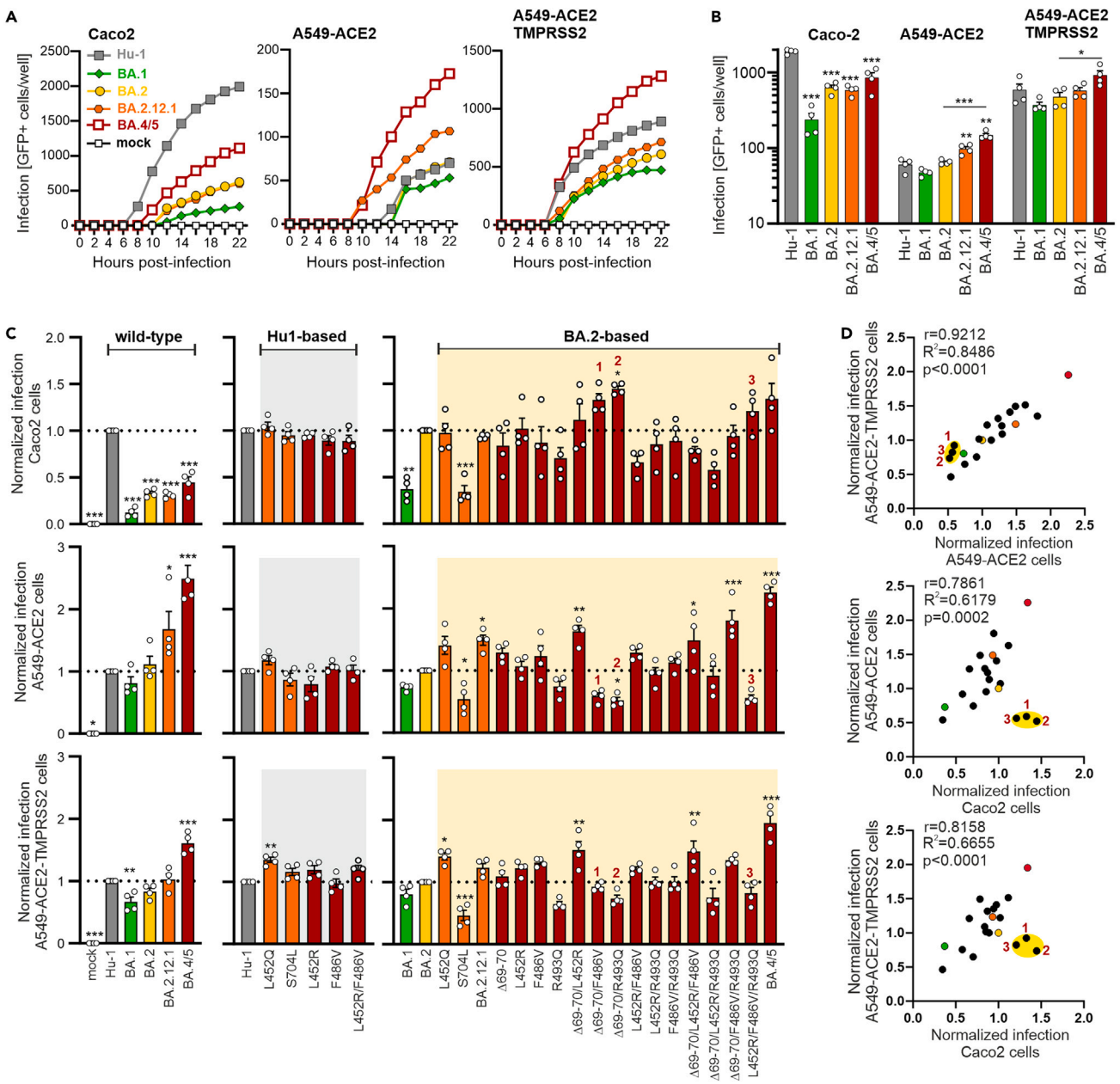

Figure 2. Impact of BA.2.12.1 and BA.4/5 mutations on Spike-mediated infection

(A) Infection kinetics of Caco2, A549-ACE2, and A549-ACE2-TMPRSS2 cells infected by VSVpp carrying the indicated mutant S proteins. Infected GFP+ cells were automatically quantified over a period of 22 h. Exemplary kinetic representing one out of four independent experiments (from Figure 2B), where each dot indicates the mean of technical duplicates.

(B) Automatic quantification of infection events by counting GFP positive cells of Caco2, A549-ACE2, and A549-ACE2-TMPRSS2 cells infected by VSVpp carrying SARS-CoV-2 Spike protein of Hu-1 (gray), BA.1 (light green), BA.2 (yellow), BA.2.12.1 (orange), or BA.4/5 (dark red). Bars represent the mean of four independent experiments (±SEM). Statistical significance was tested by one-way ANOVA. *$p < 0.05$; **$p < 0.01$; ***$p < 0.001$.

(C) Automatic quantification of infection events of Caco2 (upper panel), A549-ACE2 (middle panel), and A549-ACE2-TMPRSS2 (lower panel) cells transduced with VSVΔG-GFP pseudotyped with SARS-CoV-2 S of Hu-1 (gray), BA.1 (light green), BA.2 (yellow), BA.2.12.1 (orange), or BA.4/5 (dark red) or indicated mutant S proteins. Graphs in the center show Hu-based S mutants, infection events are normalized on the Hu-1 S (set at 1) and p values indicate difference to the Hu-1 S. Graphs on the right show BA.2-based S mutants and infection events are normalized on the BA.2 S (set at 1) and p values indicate difference to the BA.2 S. Bars represent the mean of four independent experiments (±SEM). Statistical significance was tested by one-way ANOVA. *$p < 0.05$; **$p < 0.01$; ***$p < 0.001$.

(D) Correlation of the pseudotype infection events of the wild-type S or indicated mutant S proteins in A549-ACE2-TMPRSS2/A549-ACE2 (upper panel), A549-ACE2/Caco2 (middle panel), and A549-ACE2-TMPRSS2/Caco2 (lower panel) cells. Each symbol represents the average value derived from four infection experiments (shown in Figure 2C). Numbers indicate the combined mutations of BA.4/5 S proteins whose infection events do not correlate between A549 and Caco2 cells. Coefficient of correlation (r), coefficient of determination (R^2-values) and two tailed p values are provided (see also Figure S2).

impact of the R493Q change seems to be context-dependent since it increased rather than reduced infection in the presence of the Δ69-70/F486V mutations (Figure 2C). This may explain why the reversion of R493Q occurred in conjunction with other changes in BA.4/5 S proteins.

In contrast to S704L, the remaining BA.2.12.1 defining mutation L452Q moderately increased S-mediated infection and BA.2.12.1 S showed similar or slightly increased activity compared to BA.2 S (Figures 2A–2C and S2A). BA.4/5 S was efficiently expressed, processed, and incorporated into VSVpp and consequently ~2-fold more infectious than BA.2 S in A549 cells. While none of the individual mutations had significant effects, combined changes of Δ69-70/L452R, Δ69-70/L452R/F486V, or Δ69-70/F486V/R493Q increased BA.2 S-mediated infection of both A549 cell lines by 50–80% (Figure 2C). Despite ~10-fold differences in absolute entry efficiencies, the relative levels of infection mediated by genuine and mutant Omicron S proteins correlated very well between A459-ACE2 and A549-ACE2-TMPRSS2 cells (Figure 2D). Infection efficiencies of most S proteins in both A549 cell lines also correlated with those measured in Caco2 cells. However, there were three outliers: combined mutations of Δ69-70/F486V, Δ69-70/R493Q, and L452R/F486V/R493Q enhanced infection of Caco2 cells but reduced infection of A549 cells, irrespectively of TMPRSS2 overexpression (Figures 2C and 2D). The reasons for this remain to be determined, but it has been reported that these cell lines differ in their innate immune response to infection[36] and in the expression of vimentin proposed to act as SARS-CoV-2 co-receptor.[37] Taken together, a combination of BA.4/5 defining mutations was required to significantly increase BA.2 S-mediated infection efficiencies.

Impact of BA.4/5 defining mutations in S on cell-to-cell fusion

SARS-CoV-2 also spreads by direct cell-to-cell fusion and this mechanism may help the virus to evade the host immune response.[38,39] To further determine the impact of BA.2.12.1 and BA.4/5 defining mutations on S function, we performed cell-to-cell fusion assays in HEK293T cells stably expressing GFP1-10/11.[40] HEK293T cells carrying the GFP-split complementation system, in which two cells separately produce half of the reporter protein, produce GFP only upon cell-to-cell fusion, thereby generating GFP-expressing syncytia.[40] The Hu-1 S protein was most active in mediating cell-to-cell fusion and consistent with previous reports,[18,23–25] BA.4/5 S was ~5-fold more potent than BA.2 S (Figure S2C). Essentially all mutations enhanced syncytia formation by Hu-1 and BA.2 S. Our results thus add to the evidence that L452R/Q mutations increase SARS-CoV-2 fusogenicity.[18,29,41] Combined mutations of Δ69-70/L452R and L452R/F486V/R493Q had the strongest effect and rendered BA.2 S at least as active as BA.4/5 S (Figure S2C). The effects of the mutations on cell-to-cell fusion were stronger than on S-mediated infection and both functions did not correlate significantly (Figure S2D). Similar to the results obtained in VSVpp infection assays, however, combinations of changes were required to achieve fusion activities as high as the BA.4/5 S.

Mutations characteristic for BA.4/5 S reduce TMPRSS2 dependency

SARS-CoV-2 infection requires proteolytic cleavage of Spike at the S2′ site (Figure 1D) either by TMPRSS2 at the cell surface or by cathepsin B or L in endosomes.[42] Thus, it has been proposed that SARS-CoV-2 primarily enters cells at the plasma membrane in cells expressing high levels of TMPRSS2, while the endosomal pathway dominates in the absence of TMPRSS2.[6] However, it has been debated whether Omicron variants may depend less on TMPRSS2 and enter cells mainly using the cathepsin-dependent pathway.[43–46] To address this, we infected HEK293T cells stably expressing ACE2 and transiently transfected with TMPRSS2 or cathepsin expression constructs with VSVpp carrying Hu-1-based S proteins containing mutations found in BA.1 and/or BA.2 S (K417N, H655Y, N679K, and L981F), as well as those characteristic for BA.2.12.1 or BA.4/5 S. Western blot and quantitative PCR analyses confirmed the expected differences in ACE2 and TMPRSS2 expression and showed that all cell lines express cathepsin L (Figures S3A and S3B). In agreement with previous data,[47,48] mutation of H655Y near the S2′cleavage site strongly increased infection of HEK293T cells overexpressing ACE2 alone or together with cathepsins but not in those overexpressing TMPRSS2 (Figure 3A). BA.4/5 S was generally about as active as the Hu-1-H655Y S (Figures 3A and 3B). Notably, only H655Y in Hu-1 S enhanced infection in such an efficient and cathepsin-specific manner. BA.1, BA.2, and BA.2.12.1 S proteins were less (TMPRSS2) or equally (ACE2 alone or plus cathepsins) active as Hu-1 S, although all of them contain the H655Y mutation (Figure 3B). Mutation of F486V alone or together with others increased and R493Q reduced the efficiency of BA.2 S-mediated infection irrespective of TMPRSS2 or cathepsin overexpression (Figure 3A). Relative entry efficiencies of all S proteins in HEK293T cells expressing ACE2 alone or together with cathepsins correlated almost perfectly (Figure 3B). In comparison, two clusters were observed in cells overexpressing TMPRSS2 indicating that Hu-1 S and mutants thereof were more active than BA.2 S and its derivatives in the presence of high levels of TMPRSS2 (Figure 3B). However, BA.1 S was among the least and BA.4/5 S among the most active S proteins, irrespective of TMPRSS2 and cathepsin overexpression, with BA.2 S and mutants thereof showing intermediate phenotypes.

Since HEK293T cells represent a useful but artificial experimental system, we challenged the results in the A549-ACE2 lung cell line. Mutation of H655Y again strongly enhanced Hu-1 S-mediated infection, while changes of N440K, N679K, and L981F impaired it (Figures 3C and 3D). While absolute infection levels varied, relative entry efficiencies correlated well between A549 cells overexpressing TMPRSS2 or not (Figure 3E). To further address potential differences in entry pathways, we determined the impact of the TMPRSS2 inhibitor camostat and the cathepsin inhibitor E64d on infection. Camostat reduced infection of A549-ACE2-TMPRSS2 cells by VSVpp containing Hu-1 and K417N S more efficiently than those containing the various Omicron S proteins or the H655Y Hu-1 S (Figure 3F). Conversely, E64d had no effect on Hu-1 and K417N S-mediated entry but inhibited infection mediated by Omicron S proteins. In agreement with previous data,[24] susceptibility to E64d was conferred by the H655Y mutation. Both BA.2 and BA.4/5 S were more sensitive to E64d than BA.1 (Figure 3F). Surprisingly, however, camostat efficiently inhibited entry mediated by all S proteins into Caco2 cells, while E64d generally had no effect (Figure 3F). Notably, this was also the case for the three outlier mutant S proteins displaying increased infection of Caco2 cells (Figure 2D) showing that this was not due to cathepsin usage in this cell line (Figure S3D). Thus, despite higher levels of TMPRSS2 expression (Figure S3B), the H655Y, BA.1, BA.2,

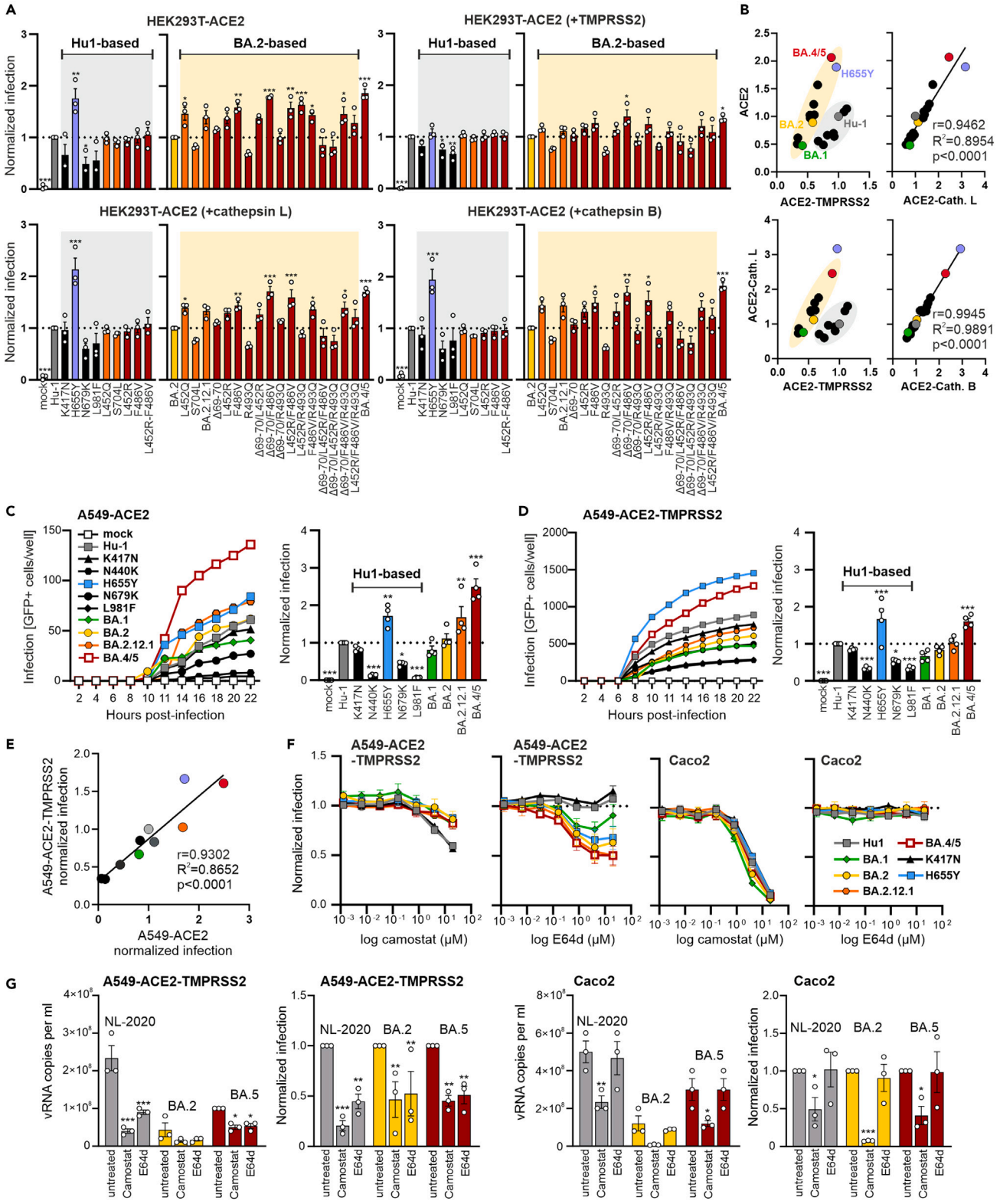

Figure 3. Impact of BA.2.12.1 and BA.4/5 mutations on TMPRSS2 dependency

(A) Automatic quantification of infection events HEK293T-ACE2 cells alone or transfected with TMPRSS2, cathepsin L or B, and infected with VSVpp carrying SARS-CoV-2 S of Hu-1 (gray), BA.1 (light green), BA.2 (yellow), BA.2.12.1 (orange), or BA.4/5 (dark red) or indicated mutant S proteins. The left part of the

Figure 3. *Continued*

graphs shows Hu-based S mutants, infection events are normalized on the Hu-1 S (set at 1) and p values indicate difference to the Hu-1 S. Graphs on the right show BA.2-based S mutants and infection events are normalized to BA.2 S (set to 1) and p values indicate difference to the BA.2 S. Bars represent the mean of three independent experiments (±SEM). Statistical significance was tested by one-way ANOVA. *p < 0.05; **p < 0.01; ***p < 0.001.

(B) Correlation of VSVpp infection events of the wild-type S or indicated mutant S proteins in HEK293T overexpressing ACE2 alone or together with TMPRSS2 or cathepsins. Each dot represents the average value derived from three infection experiments (shown in Figure 3A). Coefficient of correlation (r), coefficient of determination (R^2-values), and two tailed p values are provided.

(C) Infection kinetics (left panel) or infection events (right panel) of A549-ACE2 cells infected by VSVpp containing wild type or mutant Hu-based S proteins. The left panel shows an exemplary kinetic representing one out of three independent experiments (from right panel), where each dot indicates the mean of technical duplicates. In the bar diagram, infection events are normalized on the Hu-1 S (set at 1) and p values indicate difference to the Hu-1 S. Bars represent the mean of three independent experiments (±SEM). Statistical significance was tested by one-way ANOVA. *p < 0.05; **p < 0.01; ***p < 0.001.

(D) Infection kinetics (left panel) or infection events (right panel) of A549-ACE2-TMPRSS2 cells infected by VSVpp containing the wild type or the indicated Hu-based S proteins. The left panel shows an exemplary kinetic representing one out of three independent experiments (from right panel), where each dot indicates the mean of technical duplicates. In the bar diagram, infection events are normalized on the Hu-1 S (set at 1) and p values indicate difference to the Hu-1 S. Bars represent the mean of three independent experiments (±SEM). Statistical significance was tested by one-way ANOVA. *p < 0.05; **p < 0.01; ***p < 0.001.

(E) Correlation of the pseudotype infection events of the wild-type S or indicated Hu-based mutant S proteins harboring mutations characteristic of BA.1 and/or BA.2 S in A549 overexpressing ACE2 alone/with TMPRSS2. Each dot represents the average value derived from three infection experiments (shown in Figures 3C and 3D). Coefficient of correlation (r), coefficient of determination (R^2-values) and two tailed p values are provided.

(F) Automated quantification of GFP fluorescence of A549-ACE2-TMPRSS2 (left panel) or Caco2 (right panel) cells infected with VSVΔG-GFP pseudotyped with the indicated S variants. Cells were pre-treated (1 h, 37°C) with 20 μM of camostat or E64d in the highest concentration and diluted in a 1:5 titration row. Symbols represent the mean of three independent experiments (±SEM).

(G) Quantification of viral N RNA levels in the supernatant of A549-ACE2-TMPRSS2 (left panel) and Caco2 (right panel) cells infected with the indicated SARS-CoV-2 variants (MOI = 0.05), collected at 48 h post-infection. Cells were pre-treated (1 h, 37°C) with 20 μM of camostat or E64d. The right graph of each panel shows the reduction of vRNA levels in the supernatants relative to the untreated control (set at 1). Bars represent the mean of three independent experiments (±SEM). Non-infected controls were below the quantification level (<1000). Statistical significance was tested by two-way ANOVA. *p < 0.05; **p < 0.01; ***p < 0.001. See also Figure S3.

BA.2.12.1, and BA.4/5 S proteins also used cathepsins for infection of A549-ACE2-TMPRSS2 cells but entered Caco2 cells exclusively by the TMPRSS2 dependent pathway. Our results are contradictory to previous studies reporting that E64d inhibits infection mediated by S proteins containing the H655Y mutation in Caco2 cells.[47,49] To further address this, we performed infection experiments using three genuine SARS-CoV-2 variants, i.e., the early NL-2020 strain, BA.2, and BA.5. Similarly to the results obtained using S containing VSVpp, both camostat and E64d inhibited the three SARS-CoV-2 variants in A549-ACE2-TMPRSS2 cells, while only camostat showed significant inhibitory effects in Caco2 cells. Altogether, BA.1 S was attenuated regardless of the entry protease. BA.4/5 S allowed cathepsin-dependent infection of A549-ACE2-TMPRSS2 cells. However, in some cell types (e.g., Caco2) TMPRSS2 is essential for infection, which agrees with the finding that TMPRSS2 is generally critical for SARS-CoV-2 murine airway infection *in vivo*.[44,46]

Impact of BA.2.12.1 and BA.4/5 defining mutations on neutralization

Recent studies reported that the Omicron BA.2.12.1 and BA.4/5 S show even lower sensitivity to vaccine-induced or therapeutic neutralizing Abs than the original BA.2 S.[21,45] To determine the contribution of individual mutations to improved immune evasion, we analyzed the sensitivity of 17 Hu-1- or BA.2-based mutant S proteins to neutralization by sera from two individuals who received the heterologous ChAdOx1-nCoV-19/BNT162b2 vaccination and two individuals who received a prime boost vaccination with the mRNA-based BioNTech-Pfizer (BNT162b2) vaccine. The neutralizing capacity of the four sera varied and serum of donor 4 was inactive against BA.2 (Figure 4A). In agreement with published data,[9,50–52] the sera showed ∼2- to >10-fold lower efficiency against BA.2 S than against Hu-1 S (Figures 4A, 4B, S4A, and S4B). As expected,[18,21,53] mutations of L452Q/R reduced Hu-1 S sensitivity to neutralization ∼2-fold, while S704L increased susceptibility. BA.4/5 S was 1.4- to 6.8-fold less sensitive than BA.2 S and mutation of L452R alone or in combination with F486V contributed to reduced sensitivity to neutralization. In contrast, reversion of R493Q alone or in combination with other changes increased neutralization sensitivity (Figures 4B and S4B). This is conceivable since 493Q is present in the early S protein used for vaccination of the participants of the present study. Thus, the Q493R change most likely emerged in Omicron BA.1 and BA.2 VOCs because it promoted evasion of humoral immune responses induced by early SARS-CoV-2 strains and COVID-19 vaccines or monoclonal antibodies.[54] Later it may have reverted in BA.4/5 to evade immunity induced by BA.1/2 infection and because other changes were sufficient to confer resistance to humoral immune responses. Notably, the ability of the sera to neutralize specific S proteins was donor dependent. For example, serum from donor 1 neutralized BA.2.12.1 with higher efficiency than BA.2, while the opposite was observed for donor 3. Efficient immune evasion of BA.1 S most likely came at the cost of reduced infectivity.[10,17] However, we identified positive correlations between the ability of BA.2-based mutant S proteins to mediate infection and to reduce the sensitivity to neutralization by sera from two donors (Figure S4C). Thus, BA.4/5 defining mutations seem to promote both efficient infection and humoral immune evasion.

Finally, we examined the impact of specific mutations in Hu-1 and BA.2 S on neutralization by FDA-approved therapeutic monoclonal antibodies bamlanivimab, casivirimab, imdevimab, and bebtelovimab. Predictably,[21,31,55,56] the BA.2 VOC was not inhibited by bamlanivimab and casivirimab and mutation of L452R and F486V in Hu-1 S were sufficient for full resistance to neutralization respectively by bamlanivimab and casivirimab (Figures 4C and S4D). In comparison, R493Q slightly sensitized BA.2 to neutralization by casivirimab. As previously reported,[21,55] BA.2, BA.2.12.1 as well as BA.4/5 S maintained some susceptibility to imdevimab, although the IC_{50} was ∼30- to 40-fold higher compared to Hu-1 S. In agreement with published data,[21,31,55,57] bebtelovimab was active against all SARS-CoV-2 VOCs analyzed, including

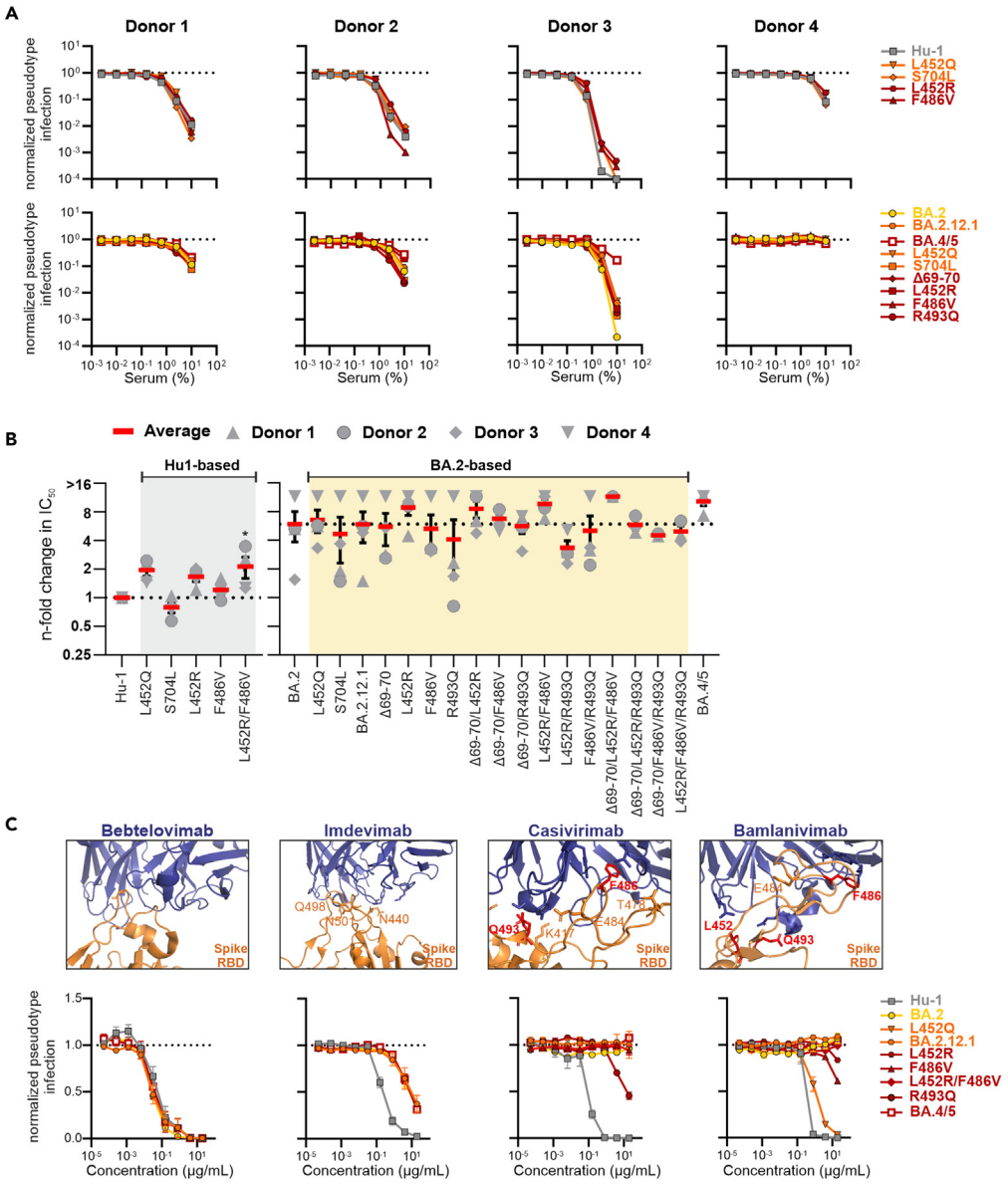

Figure 4. Impact of mutations in the Omicron BA.2.12.1 and BA.4/5 Spike on neutralization by sera and therapeutic Abs

(A) Neutralization of VSVpp carrying the indicated wild type and mutant S proteins by sera obtained from two AZN/BNT (left panel) and two BNT/BNT (right panel) vaccinated individuals compared to the untreated control (set to one). Infection was measured in Caco2 cells. Symbols represent the mean of technical duplicates. In the upper panel the Hu-based S variants are indicated while in the lower panel the BA.2-based variants.

(B) Changes in TCID50 values obtained for neutralization of the indicated mutant Hu-based (left panel) or BA.2-based (right panel) S proteins by sera from four vaccinated individuals relative to those obtained for the Hu-1 S. Symbols indicate individual donors and solid red bars indicate average values (±SEM) for the four sera.

(C) Close-up view of neutralizing antibodies binding the SARS-CoV-2 Spike (PDB: 7MMO; 6XDG; 7KMG), as indicated) and automated quantification of infection events of Caco2 cells transduced with VSVΔG-GFP pseudotyped with the indicated S variants. VSVpp were pre-treated (30 min, RT) with the indicated amounts of bebtelovimab, ikmdevimab, casivirimab, or bamlanivimab. Symbols represent the mean of three independent experiments (±SEM). (see also Figure S4).

BA.4/5 (Figure 4C). Altogether, our results support that the impact of individual mutations on neutralization sensitivity varies strongly between sera from vaccinated individuals and reveal the individual mutations that mediate efficient evasion of therapeutic antibodies.

DISCUSSION

Mutations in the S protein govern the ability of SARS-CoV-2 VOCs to evade humoral immune responses, use proteases as entry co-factors and infect cells.[5] Expanding previous studies,[18,21,24,25,41,41,55] we systematically analyzed the functional impact of individual and combined

mutations in the S proteins of SARS-CoV-2 Omicron subvariants BA.2.12.1 and BA.4/5 that dominated the COVID-19 pandemic in the second half of 2022 (Figure 1B). BA.2.12.1 S was equally (Caco2 cells) or moderately more (1.2– to 1.5-fold in A549 cells) infectious than the S protein of the parental BA.2 VOC and mediated ~2-fold higher levels of syncytia. In comparison, the S protein of BA.4/5 was generally more active in mediating infection (1.3- to 2.3-fold; (Figure 2C) and syncytia formation (~5-fold) compared to BA.2 S (Figure S2C). Thus, it is conceivable that BA.4/5 outcompeted BA.2 and BA.2.12.1 because of both increased resistance to neutralization[19,21,24,31,45] and higher infectivity. Our results agree with evidence that BA.5 displays higher replication fitness, transmissibility, and pathogenicity compared to BA.2.[17,18,23–25,45,58] Our data further show that individual mutations had only modest enhancing (Δ69-70, L452Q/R, and F486V) or attenuating (R493Q and S704L) effects on BA.2 S-mediated VSVpp infection (Figure 2C). Essentially all BA.2.12.1 and BA.4/5 defining mutations, however, increased syncytia formation (Figure S2C) suggesting that emerging Omicron VOCs might spread more efficiently by direct cell-to-cell contact than previous SARS-CoV-2 variants. Notably, combinations of Δ69-70, L452R, and/or F486V mutations enhanced BA.2 S function more efficiently (infection up to 80% and cell-to-cell fusion up to 8-fold) than any individual changes. However, the BA.4/5 S was generally more active in mediating infection than all mutant S proteins supporting that the combination of all four BA.4/5 S defining mutations is required for full activity.

Some of our results seem at odds with published data. For example, it has been proposed that the F486V mutation facilitates immune escape but may compromise S affinity for ACE2,[21,59] while the R493Q reversion may restore receptor affinity and consequently infectivity of BA.4/5.[21] We found, however, that the single F486V change enhanced infection of all cell types analyzed (except Caco2) by 20–60%, while mutation of R493Q generally reduced BA.2 S-mediated infection by 25–40% (summarized in Figure S3C). In addition, BA.2 S containing combined mutations of F486V/R493Q was not more infectious than S containing the F486V mutation alone. Altogether, our results suggest that F486V rather than R493Q contributes to the higher infectivity of BA.4/5 S. Apparent discrepancies may in part result from different experimental approaches. Our approach allows to determine the levels of S bound to ACE2 but not to quantify the binding affinities. The previous conclusion that F486V may reduce and R493Q enhance S affinity for ACE2 was based on sensitivity of VSVpp to neutralization by dimeric hACE2 *in vitro*, molecular modeling, and affinity measurements using purified RBD domain or Spike proteins.[21,32,60] ACE2 binding is only the first step of the S-mediated infection process and we observed the enhancing effect of F486V and reducing effect of R493Q on S-mediated VSVpp infection using different target cells lines. Notably, mutation of F486P seems to play a key role in the increased infectivity, transmissibility, and immune escape ability of the currently (May 2023) dominating Omicron XBB.1.5 subvariant.[24,61] It has recently been reported that the L452R mutation, which is present in the Delta and BA.5 variants but absent in BA.1 and BA.2 (2.75, Ca.1/7, BS.1BA.5, CK2.1, XAY, XBA) increases SARS-CoV-2 fusogenicity and infectivity by enhancing proteolytic cleavage of the S protein.[29] In addition, introduction of L452R in BA.1 S promoted SARS-CoV-2 replication in humanized ACE2 mice.[41] We did not observe a significant effect of L452R on S processing Figure S1A) but mutations of L452Q/R enhanced BA.2 S-mediated cell-to-cell fusion (Figure S2C) and infection of A549 cells (Figure 2C). Effects in single-round VSVpp infection assays were modest but may be amplified over multiple rounds of replication in the context of infectious SARS-CoV-2 variants.

We found that the activity of Omicron S proteins in mediating infection and cell-to-cell fusion gradually increased, with BA.1<BA.2< BA.2.12.1<BA.4/5, reflecting their order of appearance and/or dominance in the human population. However, this sequential increase in S-mediated infection was observed irrespective of the levels of ACE2 and TMPRSS2 in the viral target cells and associated with efficient processing and incorporation of BA.4/5 S into VSVpp. It has been reported that Omicron BA.1 prefers cathepsin L over TMPRSS2 for infection[43,49,62] and suggested that inefficient utilization of TMPRSS2 may explain its poor infectivity for primary lung cells in murine models.[44] We found that the activity of BA.4/5 S compared to BA.2 S is only ~1.3-fold higher in cells expressing high levels of TMPRSS2 but ~2-fold higher in cells expressing higher levels of cathepsin (Figure S3C). BA.1 S was generally less active than Hu-1 S, irrespectively of the levels of TMPRSS2 and cathepsin L expression. Notably, Omicron variants and the Hu-1-H655Y mutant S preferentially used cathepsin for infection of A549-ACE2-TMPRSS2 cells but only TMPRSS2 in Caco2 cells, despite efficient expression of cathepsin L. The latter was confirmed using genuine SARS-CoV-2 variants (Figure 3G). Thus, Omicron VOCs are more prone to use cathepsins than the early SARS-CoV-2 Hu-1 variant but utilization seems to depend on the target cell type rather than TMPRSS2 expression levels.

In conclusion, each successive Omicron subvariant that outcompeted the previous one has apparently not only become better in antibody evasion but also more infectious and hence most likely more transmissible. Notably, convergent evolution is common and mutations at several sites analyzed in the present study, e.g., L452R/Q/M, F486V/P/S, and the R493Q reversion, are found in distinct SARS-CoV-2 lineages. It seems that currently, mainly new Omicron variants emerge by recombination and antigenic drift.[63] However, the Omicron VOC containing an unusually high number of mutations in S initially emerged unexpectedly.[4] The frequency of specific mutations in dominating SARS-CoV-2 VOCs fluctuates (Figure 1B) and changes that are advantageous for efficient viral infection or immune evasion may re-emerge in future variants. To assess not only the immune evasion capacity but also transmissibility and replication fitness of new variants, it will thus be important to further define the role of specific amino acid position on Spike function.

Limitations of the study

We used pseudotyped viral particles instead of replication-competent recombinant SARS-CoV-2 variants in most experiments. To assess overall effects on S function, we did not normalize for the same levels of surface S proteins in the cell-to-cell fusion assays. Thus, besides fusogenicity alterations in expression levels and/or localization of S might impact the results. However, the latter effects are most likely minor since we observed little variation in S expression levels and localization in transfected HEK293T cells. To reduce the risk for artifacts, we used Spike proteins lacking an artificial deletion of the C-terminal ER-retention motif that is often used to increase SARS-CoV-2 pseudoparticle infectivity for *in vitro* assays. Nonetheless, the Spike-containing VSVpp does not fully recapitulate the properties of genuine SARS-CoV-2

particles. Since our focus was on functional analyses, we examined only a limited number of sera from vaccinated individuals. Finally, the impact of some amino acid changes might be context-dependent and this may explain why some individual changes had disruptive effects on Hu-1 and/or BA.2 S function although they are found e.g., in Omicron BA.4/5 S proteins.

STAR★METHODS

Detailed methods are provided in the online version of this paper and include the following:

- KEY RESOURCES TABLE
- RESOURCE AVAILABILITY
  - Lead contact
  - Materials availability
  - Data and code availability
- EXPERIMENTAL MODEL AND SUBJECT DETAILS
  - Cells
  - Sera from vaccinated individuals
  - Viruses
  - Expression constructs
- METHOD DETAILS
  - Molecular images
  - Analysis of sequences over time
  - Pseudoparticle Production
  - Pseudovirus infection
  - Pseudoparticle inhibition
  - Virus treatment
  - qRT-PCR of supernatants
  - qRT-PCR of cells
  - Whole-cell and cell-free lysates
  - SDS-PAGE and immunoblotting
  - ACE2 interaction assay
  - GFP-split fusion assay
- QUANTIFICATION AND STATISTICAL ANALYSIS
  - Statistical analysis

SUPPLEMENTAL INFORMATION

Supplemental information can be found online at https://doi.org/10.1016/j.isci.2023.108299.

ACKNOWLEDGMENTS

We thank Kerstin Regensburger, Regina Burger, Jana-Romana Fischer, Birgit Ott, Martha Meyer, Nicola Schrott, and Daniela Krnavek for technical assistance. The ACE2 expression vector plasmid was kindly provided by Shinji Makino. The SARS-CoV-2 S expression plasmids and the A549-ACE2/-TMPRSS2 were kindly provided Stefan Pöhlmann. HEK293T-GFP$_{1-10/11}$ were kindly provided by Olivier Schwartz. Vero E6-ACE2-TMPRSS2 cells were kindly provided by Viviana Simon. C.P. and S.N. are part of the International Graduate School for Molecular Medicine (IGradU). This study was supported by DFG grants to F.K. (CRC 1279 and SPP 1923), K.M.J.S. (CRC 1279, SPP 1923, and SP 1600/6-1). F.K. and K.M.J.S. were supported by the BMBF (Restrict SARS-CoV-2 and IMMUNOMOD).

AUTHOR CONTRIBUTIONS

C.P. performed most experiments with support by S.N, R.N., and F.Z., K.M.J.S., and F.K. conceived the study and planned experiments. F.K. wrote the initial draft of the manuscript. All authors reviewed and approved the manuscript.

DECLARATION OF INTERESTS

All authors declare no competing interests.

Received: May 30, 2023
Revised: September 4, 2023
Accepted: October 19, 2023
Published: October 27, 2023

REFERENCES

1. Gorbalenya, A.E., Enjuanes, L., Ziebuhr, J., and Snijder, E.J. (2006). Nidovirales: Evolving the largest RNA virus genome. Virus Res. *117*, 17–37. https://doi.org/10.1016/j.virusres.2006.01.017.
2. Robson, F., Khan, K.S., Le, T.K., Paris, C., Demirbag, S., Barfuss, P., Rocchi, P., and Ng, W.-L. (2020). Coronavirus RNA Proofreading: Molecular Basis and Therapeutic Targeting. Mol. Cell *79*, 710–727. https://doi.org/10.1016/j.molcel.2020.07.027.
3. Markov, P.V., Ghafari, M., Beer, M., Lythgoe, K., Simmonds, P., Stilianakis, N.I., and Katzourakis, A. (2023). The evolution of SARS-CoV-2. Nat. Rev. Microbiol. *21*, 361–379. https://doi.org/10.1038/s41579-023-00878-2.
4. Jung, C., Kmiec, D., Koepke, L., Zech, F., Jacob, T., Sparrer, K.M.J., and Kirchhoff, F. (2022). Omicron: what makes the latest SARS-CoV-2 variant of concern so concerning? J. Virol. *96*, jvi0207721. https://doi.org/10.1128/jvi.02077-21.
5. Carabelli, A.M., Peacock, T.P., Thorne, L.G., Harvey, W.T., Hughes, J., COVID-19 Genomics UK Consortium, Peacock, S.J., Barclay, W.S., de Silva, T.I., Towers, G.J., and Robertson, D.L. (2023). SARS-CoV-2 variant biology: immune escape, transmission and fitness. Nat. Rev. Microbiol. *21*, 162–177. https://doi.org/10.1038/s41579-022-00841-7.
6. Hoffmann, M., Kleine-Weber, H., Schroeder, S., Krüger, N., Herrler, T., Erichsen, S., Schiergens, T.S., Herrler, G., Wu, N.-H., Nitsche, A., et al. (2020). SARS-CoV-2 Cell Entry Depends on ACE2 and TMPRSS2 and Is Blocked by a Clinically Proven Protease Inhibitor. Cell *181*, 271–280.e8. https://doi.org/10.1016/j.cell.2020.02.052.
7. Letko, M., Marzi, A., and Munster, V. (2020). Functional assessment of cell entry and receptor usage for SARS-CoV-2 and other lineage B betacoronaviruses. Nat. Microbiol. *5*, 562–569. https://doi.org/10.1038/s41564-020-0688-y.
8. Andrews, N., Stowe, J., Kirsebom, F., Toffa, S., Rickeard, T., Gallagher, E., Gower, C., Kall, M., Groves, N., O'Connell, A.-M., et al. (2022). Covid-19 vaccine effectiveness against the Omicron (B.1.1.529) variant. N. Engl. J. Med. *386*, 1532–1546. https://doi.org/10.1056/NEJMoa2119451.
9. Cele, S., Jackson, L., Khoury, D.S., Khan, K., Moyo-Gwete, T., Tegally, H., San, J.E., Cromer, D., Scheepers, C., Amoako, D.G., et al. (2022). Omicron extensively but incompletely escapes Pfizer BNT162b2 neutralization. Nature *602*, 654–656. https://doi.org/10.1038/s41586-021-04387-1.
10. Hoffmann, M., Krüger, N., Schulz, S., Cossmann, A., Rocha, C., Kempf, A., Nehlmeier, I., Graichen, L., Moldenhauer, A.-S., Winkler, M.S., et al. (2022). The Omicron variant is highly resistant against antibody-mediated neutralization: implications for control of the COVID-19 pandemic. Cell *185*, 447–456.e11. https://doi.org/10.1016/j.cell.2021.12.032.
11. Yamasoba, D., Kimura, I., Nasser, H., Morioka, Y., Nao, N., Ito, J., Uriu, K., Tsuda, M., Zahradnik, J., Shirakawa, K., et al. (2022). Virological Characteristics of SARS-CoV-2 BA.2 Variant. Cell *185*, 2103–2115.e19. https://doi.org/10.1101/2022.02.14.480335.
12. Suzuki, R., Yamasoba, D., Kimura, I., Wang, L., Kishimoto, M., Ito, J., Morioka, Y., Nao, N., Nasser, H., Uriu, K., et al. (2022). Attenuated fusogenicity and pathogenicity of SARS-CoV-2 Omicron variant. Nature *603*, 700–705. https://doi.org/10.1038/s41586-022-04462-1.
13. Pastorio, C., Zech, F., Noettger, S., Jung, C., Jacob, T., Sanderson, T., Sparrer, K.M.J., and Kirchhoff, F. (2022). Determinants of Spike infectivity, processing, and neutralization in SARS-CoV-2 Omicron subvariants BA.1 and BA.2. Cell Host Microbe *30*, 1255–1268.e5. https://doi.org/10.1016/j.chom.2022.07.006.
14. Wolf, K.A., Kwan, J.C., and Kamil, J.P. (2022). Structural Dynamics and Molecular Evolution of the SARS-CoV-2 Spike Protein. mBio *13*, e0203021. https://doi.org/10.1128/mbio.02030-21.
15. Gobeil, S.M.-C., Henderson, R., Stalls, V., Janowska, K., Huang, X., May, A., Speakman, M., Beaudoin, E., Manne, K., Li, D., et al. (2022). Structural diversity of the SARS-CoV-2 Omicron spike. Mol. Cell *82*, 2050–2068.e6. https://doi.org/10.1016/j.molcel.2022.03.028.
16. Neerukonda, S.N., Wang, R., Vassell, R., Baha, H., Lusvarghi, S., Liu, S., Wang, T., Weiss, C.D., and Wang, W. (2022). Characterization of Entry Pathways, Species-Specific Angiotensin-Converting Enzyme 2 Residues Determining Entry, and Antibody Neutralization Evasion of Omicron BA.1, BA.1.1, BA.2, and BA.3 Variants. J. Virol. *96*, e0114022. https://doi.org/10.1128/jvi.01140-22.
17. Nchioua, R., Diofano, F., Noettger, S., von Maltitz, P., Stenger, S., Zech, F., Münch, J., Sparrer, K.M.J., Just, S., and Kirchhoff, F. (2022). Strong attenuation of SARS-CoV-2 Omicron BA.1 and increased replication of the BA.5 subvariant in human cardiomyocytes. Sig. Transduct Target Ther. *7*, 395–403. https://doi.org/10.1038/s41392-022-01256-9.
18. Kimura, I., Yamasoba, D., Tamura, T., Nao, N., Suzuki, T., Oda, Y., Mitoma, S., Ito, J., Nasser, H., Zahradnik, J., et al. (2022). Virological characteristics of the SARS-CoV-2 Omicron BA.2 subvariants, including BA.4 and BA.5. Cell *185*, 3992–4007.e16. https://doi.org/10.1016/j.cell.2022.09.018.
19. Tegally, H., Moir, M., Everatt, J., Giovanetti, M., Scheepers, C., Wilkinson, E., Subramoney, K., Makatini, Z., Moyo, S., Amoako, D.G., et al. (2022). Emergence of SARS-CoV-2 Omicron lineages BA.4 and BA.5 in South Africa. Nat. Med. *28*, 1785–1790. https://doi.org/10.1038/s41591-022-01911-2.
20. Xia, S., Wang, L., Zhu, Y., Lu, L., and Jiang, S. (2022). Origin, virological features, immune evasion and intervention of SARS-CoV-2 Omicron sublineages. Signal Transduct. Target. Ther. *7*, 241. https://doi.org/10.1038/s41392-022-01105-9.
21. Wang, Q., Guo, Y., Iketani, S., Nair, M.S., Li, Z., Mohri, H., Wang, M., Yu, J., Bowen, A.D., Chang, J.Y., et al. (2022). Antibody evasion by SARS-CoV-2 Omicron subvariants BA.2.12.1, BA.4 and BA.5. Nature *608*, 603–608. https://doi.org/10.1038/s41586-022-05053-w.
22. Islam, M.R., Shahriar, M., and Bhuiyan, M.A. (2022). The latest Omicron BA.4 and BA.5 lineages are frowning toward COVID-19 preventive measures: A threat to global public health. Health Sci. Rep. *5*, e884. https://doi.org/10.1002/hsr2.884.
23. Tamura, T., Ito, J., Uriu, K., Zahradnik, J., Kida, I., Anraku, Y., Nasser, H., Shofa, M., Oda, Y., Lytras, S., et al. (2023). Virological characteristics of the SARS-CoV-2 XBB variant derived from recombination of two Omicron subvariants. Nat. Commun. *14*, 2800. https://doi.org/10.1038/s41467-023-38435-3.
24. Qu, P., Faraone, J.N., Evans, J.P., Zheng, Y.-M., Carlin, C., Anghelina, M., Stevens, P., Fernandez, S., Jones, D., Panchal, A.R., et al. (2023). Enhanced evasion of neutralizing antibody response by Omicron XBB.1.5, CH.1.1, and CA.3.1 variants. Cell Rep. *42*, 112443. https://doi.org/10.1016/j.celrep.2023.112443.
25. Hoffmann, M., Wong, L.-Y.R., Arora, P., Zhang, L., Rocha, C., Odle, A., Nehlmeier, I., Kempf, A., Richter, A., Halwe, N.J., et al. (2023). Omicron subvariant BA.5 efficiently infects lung cells. Nat. Commun. *14*, 3500. https://doi.org/10.1038/s41467-023-39147-4.
26. Hadfield, J., Megill, C., Bell, S.M., Huddleston, J., Potter, B., Callender, C., Sagulenko, P., Bedford, T., and Neher, R.A. (2018). Nextstrain: real-time tracking of pathogen evolution. Bioinformatics *34*, 4121–4123. https://doi.org/10.1093/bioinformatics/bty407.
27. Riepler, L., Rössler, A., Falch, A., Volland, A., Borena, W., von Laer, D., and Kimpel, J. (2020). Comparison of Four SARS-CoV-2 Neutralization Assays. Vaccines (Basel) *9*, 13. https://doi.org/10.3390/vaccines9010013.
28. Schmidt, F.I., Lu, A., Chen, J.W., Ruan, J., Tang, C., Wu, H., and Ploegh, H.L. (2016). A single domain antibody fragment that recognizes the adaptor ASC defines the role of ASC domains in inflammasome assembly. J. Exp. Med. *213*, 771–790. https://doi.org/10.1084/jem.20151790.
29. Zhang, Y., Zhang, T., Fang, Y., Liu, J., Ye, Q., and Ding, L. (2022). SARS-CoV-2 spike L452R mutation increases Omicron variant fusogenicity and infectivity as well as host glycolysis. Sig. Transduct. Target Ther. *7*, 76–83. https://doi.org/10.1038/s41392-022-00941-z.
30. Zech, F., Schniertshauer, D., Jung, C., Herrmann, A., Cordsmeier, A., Xie, Q., Nchioua, R., Prelli Bozzo, C., Volcic, M., Koepke, L., et al. (2021). Spike residue 403 affects binding of coronavirus spikes to human ACE2. Nat. Commun. *12*, 6855. https://doi.org/10.1038/s41467-021-27180-0.
31. Cao, Y., Yisimayi, A., Jian, F., Song, W., Xiao, T., Wang, L., Du, S., Wang, J., Li, Q., Chen, X., et al. (2022). BA.2.12.1, BA.4 and BA.5 escape antibodies elicited by Omicron infection. Nature *608*, 593–602. https://doi.org/10.1038/s41586-022-04980-y.
32. Philip, A.M., Ahmed, W.S., and Biswas, K.H. (2023). Reversal of the unique Q493R mutation increases the affinity of Omicron S1-RBD for ACE2. Comput. Struct. Biotechnol. J. *21*, 1966–1977. https://doi.org/10.1016/j.csbj.2023.02.019.
33. Saviano, A., Brigida, M., Petruzziello, C., Zanza, C., Candelli, M., Morabito Loprete, M.R., Saleem, F., and Ojetti, V. (2023). Intestinal Damage, Inflammation and Microbiota Alteration during COVID-19 Infection. Biomedicines *11*, 1014. https://doi.org/10.3390/biomedicines11041014.
34. Wu, X., Jing, H., Wang, C., Wang, Y., Zuo, N., Jiang, T., Novakovic, V.A., and Shi, J. (2022). Intestinal Damage in COVID-19: SARS-CoV-2 Infection and Intestinal Thrombosis. Front. Microbiol. *13*, 860931. https://doi.org/10.3389/fmicb.2022.860931.
35. Chang, C.-W., Parsi, K.M., Somasundaran, M., Vanderleeden, E., Liu, P., Cruz, J., Cousineau,

A., Finberg, R.W., and Kurt-Jones, E.A. (2022). A Newly Engineered A549 Cell Line Expressing ACE2 and TMPRSS2 Is Highly Permissive to SARS-CoV-2, Including the Delta and Omicron Variants. Viruses *14*, 1369. https://doi.org/10.3390/v14071369.

36. Sun, G., Cui, Q., Garcia, G., Wang, C., Zhang, M., Arumugaswami, V., Riggs, A.D., and Shi, Y. (2021). Comparative transcriptomic analysis of SARS-CoV-2 infected cell model systems reveals differential innate immune responses. Sci. Rep. *11*, 17146. https://doi.org/10.1038/s41598-021-96462-w.
37. Arrindell, J., Abou Atmeh, P., Jayet, L., Sereme, Y., Mege, J.-L., and Desnues, B. (2022). Vimentin is an important ACE2 co-receptor for SARS-CoV-2 in epithelial cells. iScience *25*, 105463. https://doi.org/10.1016/j.isci.2022.105463.
38. Zeng, C., Evans, J.P., King, T., Zheng, Y.-M., Oltz, E.M., Whelan, S.P.J., Saif, L.J., Peeples, M.E., and Liu, S.-L. (2022). SARS-CoV-2 spreads through cell-to-cell transmission. Proc. Natl. Acad. Sci. USA *119*, e2111400119. https://doi.org/10.1073/pnas.2111400119.
39. Buchrieser, J., Dufloo, J., Hubert, M., Monel, B., Planas, D., Rajah, M.M., Planchais, C., Porrot, F., Guivel-Benhassine, F., Van der Werf, S., et al. (2020). Syncytia formation by SARS-CoV-2-infected cells. EMBO J. *39*, e106267. https://doi.org/10.15252/embj.2020106267.
40. Planas, D., Bruel, T., Grzelak, L., Guivel-Benhassine, F., Staropoli, I., Porrot, F., Planchais, C., Buchrieser, J., Rajah, M.M., Bishop, E., et al. (2021). Sensitivity of infectious SARS-CoV-2 B.1.1.7 and B.1.351 variants to neutralizing antibodies. Nat. Med. *27*, 917–924. https://doi.org/10.1038/s41591-021-01318-5.
41. Motozono, C., Toyoda, M., Zahradnik, J., Saito, A., Nasser, H., Tan, T.S., Ngare, I., Kimura, I., Uriu, K., Kosugi, Y., et al. (2021). SARS-CoV-2 spike L452R variant evades cellular immunity and increases infectivity. Cell Host Microbe *29*, 1124–1136.e11. https://doi.org/10.1016/j.chom.2021.06.006.
42. Jackson, C.B., Farzan, M., Chen, B., and Choe, H. (2022). Mechanisms of SARS-CoV-2 entry into cells. Nat. Rev. Mol. Cell Biol. *23*, 3–20. https://doi.org/10.1038/s41580-021-00418-x.
43. Meng, B., Abdullahi, A., Ferreira, I.A.T.M., Goonawardane, N., Saito, A., Kimura, I., Yamasoba, D., Gerber, P.P., Fatihi, S., Rathore, S., et al. (2022). Altered TMPRSS2 usage by SARS-CoV-2 Omicron impacts infectivity and fusogenicity. Nature *603*, 706–714. https://doi.org/10.1038/s41586-022-04474-x.
44. Iwata-Yoshikawa, N., Kakizaki, M., Shiwa-Sudo, N., Okura, T., Tahara, M., Fukushi, S., Maeda, K., Kawase, M., Asanuma, H., Tomita, Y., et al. (2022). Essential role of TMPRSS2 in SARS-CoV-2 infection in murine airways. Nat. Commun. *13*, 6100. https://doi.org/10.1038/s41467-022-33911-8.
45. Aggarwal, A., Akerman, A., Milogiannakis, V., Silva, M.R., Walker, G., Stella, A.O., Kindinger, A., Angelovich, T., Waring, E., Amatayakul-Chantler, S., et al. (2022). SARS-CoV-2 Omicron BA.5: Evolving tropism and evasion of potent humoral responses and resistance to clinical immunotherapeutics relative to viral variants of concern. EBioMedicine *84*, 104270. https://doi.org/10.1016/j.ebiom.2022.104270.
46. Metzdorf, K., Jacobsen, H., Greweling-Pils, M.C., Hoffmann, M., Lüddecke, T., Miller, F., Melcher, L., Kempf, A.M., Nehlmeier, I., Bruder, D., et al. (2023). TMPRSS2 Is Essential for SARS-CoV-2 Beta and Omicron Infection. Viruses *15*, 271. https://doi.org/10.3390/v15020271.
47. Yamamoto, M., Tomita, K., Hirayama, Y., Inoue, J., Kawaguchi, Y., and Gohda, J. (2022). SARS-CoV-2 Omicron Spike H655Y Mutation Is Responsible for Enhancement of the Endosomal Entry Pathway and Reduction of Cell Surface Entry Pathways. Preprint at bioRxiv *2022*. https://doi.org/10.1101/2022.03.21.485084.
48. Hu, B., Chan, J.F.-W., Liu, H., Liu, Y., Chai, Y., Shi, J., Shuai, H., Hou, Y., Huang, X., Yuen, T.T.-T., et al. (2022). Spike mutations contributing to the altered entry preference of SARS-CoV-2 omicron BA.1 and BA.2. Emerg. Microbes Infect. *11*, 2275–2287. https://doi.org/10.1080/22221751.2022.2117098.
49. Peacock, T.P., Brown, J.C., Zhou, J., Thakur, N., Sukhova, K., Newman, J., Kugathasan, R., Yan, A.W.C., Furnon, W., De Lorenzo, G., et al. (2021). The altered entry pathway and antigenic distance of the SARS-CoV-2 Omicron variant map to separate domains of spike protein.. Preprint at bioRxiv. https://doi.org/10.1101/2021.12.31.474653.
50. Collie, S., Champion, J., Moultrie, H., Bekker, L.-G., and Gray, G. (2022). Effectiveness of BNT162b2 Vaccine against Omicron Variant in South Africa. N. Engl. J. Med. *386*, 494–496. https://doi.org/10.1056/NEJMc2119270.
51. Iketani, S., Liu, L., Guo, Y., Liu, L., Chan, J.F.-W., Huang, Y., Wang, M., Luo, Y., Yu, J., Chu, H., et al. (2022). Antibody evasion properties of SARS-CoV-2 Omicron sublineages. Nature *604*, 553–556. https://doi.org/10.1038/s41586-022-04594-4.
52. Lu, L., Mok, B.W.-Y., Chen, L.-L., Chan, J.M.-C., Tsang, O.T.-Y., Lam, B.H.-S., Chuang, V.W.-M., Chu, A.W.-H., Chan, W.-M., Ip, J.D., et al. (2022). Neutralization of SARS-CoV-2 Omicron variant by sera from BNT162b2 or Coronavac vaccine recipients. Clin. Infect. Dis. *75*, e822–e826. https://doi.org/10.1093/cid/ciab1041.
53. Tan, T.S., Toyoda, M., Ode, H., Barabona, G., Hamana, H., Kitamatsu, M., Kishi, H., Motozono, C., Iwatani, Y., and Ueno, T. (2022). Dissecting Naturally Arising Amino Acid Substitutions at Position L452 of SARS-CoV-2 Spike. J. Virol. *96*. e0116222-22. https://doi.org/10.1128/jvi.01162-22.
54. Guigon, A., Faure, E., Lemaire, C., Chopin, M.-C., Tinez, C., Assaf, A., Lazrek, M., Hober, D., Bocket, L., Engelmann, I., and Alidjinou, E.K. (2022). Emergence of Q493R mutation in SARS-CoV-2 spike protein during bamlanivimab/etesevimab treatment and resistance to viral clearance. J. Infect. *84*, 248–288. https://doi.org/10.1016/j.jinf.2021.08.033.
55. Takashita, E., Yamayoshi, S., Simon, V., van Bakel, H., Sordillo, E.M., Pekosz, A., Fukushi, S., Suzuki, T., Maeda, K., Halfmann, P., et al. (2022). Efficacy of Antibodies and Antiviral Drugs against Omicron BA.2.12.1, BA.4, and BA.5 Subvariants. N. Engl. J. Med. *387*, 468–470. https://doi.org/10.1056/NEJMc2207519.
56. Uraki, R., Kiso, M., Iida, S., Imai, M., Takashita, E., Kuroda, M., Halfmann, P.J., Loeber, S., Maemura, T., Yamayoshi, S., et al. (2022). Characterization and antiviral susceptibility of SARS-CoV-2 Omicron BA.2. Nature *607*, 119–127. https://doi.org/10.1038/s41586-022-04856-1.
57. Westendorf, K., Žentelis, S., Wang, L., Foster, D., Vaillancourt, P., Wiggin, M., Lovett, E., van der Lee, R., Hendle, J., Pustilnik, A., et al. (2022). LY-CoV1404 (bebtelovimab) potently neutralizes SARS-CoV-2 variants. Cell Rep. *39*, 110812. https://doi.org/10.1016/j.celrep.2022.110812.
58. Uraki, R., Halfmann, P.J., Iida, S., Yamayoshi, S., Furusawa, Y., Kiso, M., Ito, M., Iwatsuki-Horimoto, K., Mine, S., Kuroda, M., et al. (2022). Characterization of SARS-CoV-2 Omicron BA.4 and BA.5 isolates in rodents. Nature *612*, 540–545. https://doi.org/10.1038/s41586-022-05482-7.
59. Starr, T.N., Greaney, A.J., Hannon, W.W., Loes, A.N., Hauser, K., Dillen, J.R., Ferri, E., Farrell, A.G., Dadonaite, B., McCallum, M., et al. (2022). Shifting mutational constraints in the SARS-CoV-2 receptor-binding domain during viral evolution. Science *377*, 420–424. https://doi.org/10.1126/science.abo7896.
60. Huo, J., Dijokaite-Guraliuc, A., Liu, C., Zhou, D., Ginn, H.M., Das, R., Supasa, P., Selvaraj, M., Nutalai, R., Tuekprakhon, A., et al. (2023). A delicate balance between antibody evasion and ACE2 affinity for Omicron BA.2.75. Cell Rep. *42*, 111903. https://doi.org/10.1016/j.celrep.2022.111903.
61. Parums, D.V. (2023). Editorial: The XBB.1.5 ('Kraken') Subvariant of Omicron SARS-CoV-2 and its Rapid Global Spread. Med. Sci. Monit. *29*, e939580. https://doi.org/10.12659/MSM.939580.
62. Willett, B.J., Grove, J., MacLean, O.A., Wilkie, C., De Lorenzo, G., Furnon, W., Cantoni, D., Scott, S., Logan, N., Ashraf, S., et al. (2022). SARS-CoV-2 Omicron is an immune escape variant with an altered cell entry pathway. Nat. Microbiol. *7*, 1161–1179. https://doi.org/10.1038/s41564-022-01143-7.
63. Shiraz, R., and Tripathi, S. (2023). Enhanced recombination among Omicron subvariants of SARS-CoV-2 contributes to viral immune escape. J. Med. Virol. *95*, e28519. https://doi.org/10.1002/jmv.28519.

STAR★METHODS

KEY RESOURCES TABLE

REAGENT or RESOURCE	SOURCE	IDENTIFIER
Antibodies		
Mouse monoclonal anti-V5 Spike (E9H8O)	Cell Signaling Technology	Cat#80076S; RRID: AB_2920661
Rabbit monoclonal anti-V5 Spike	Cell Signaling Technology	Cat#13202S; RRID: AB_2687461
Mouse monoclonal anti-VSV-M (23H12)	Absolute Antibody	Cat#Ab01404–2.0
Mouse monoclonal anti-beta Actin	Abcam	Cat#ab8226; RRID: AB_306371
IRDye 800CW Goat anti-Mouse IgG (H + L)	LI-COR	Cat#926–32210; RRID: AB_621842
IRDye 680CW Goat anti-Rabbit IgG (H + L)	LI-COR	Cat#925–68071; RRID: AB_2721181
Bamlanivimab	Lilly Pharma	LY-CoV555 700 mg; Lot#D336907A
Imdevimab	Roche	REGN10897 1332 mg; Lot#N7534
Casivirimab	Roche	REGN10933 1332 mg; Lot#N7533
Bebtelovimab	Cell Sciences	LY-CoV1404/LY3853113 100 µg; Cat#CPC539B
Bacterial and virus strains		
NEB® 5-alpha Competent E. coli (High Efficiency)	New England BioLabs	Cat#C2987H
XL2-Blue MRF' TM Ultracompetent cells	Agilent Technologies	Cat#200151
VSVΔG(GFP)*VSV-G	Prof. Karl-Klaus Conzelmann, Institute of Virology, LMU Munich, Germany	N/A
BetaCoV/Netherlands/01/NL/2020	European Virus Archive	N/A
B.1.1.529, BA.5	Prof. Dr. Florian Schmidt, University of Bonn	N/A
hCoV-19/USA/CO-CDPHE-2102544747/2021, lineage B.1.1.529, BA.2	BEI database	Cat#NR-56520
Biological samples		
Human sera	This study	N/A
Chemicals, peptides, and recombinant proteins		
DAPI	Sigma-Aldrich	Cat#D9542-1MG; CAS: 28718-90-3
L-Glutamine	PANBiotech	Cat#P04-80100
Penicillin-Streptomycin	PANBiotech	Cat#P06-07100
Complete ULTRA inhibitor cocktail tablet	Roche	Cat#05892791001
2-Mercaptoethanol	Sigma-Aldrich	Cat#M6250-100ML
Polyethyleneimine (PEI)	Sigma-Aldrich	Cat#408727-100ML
4% Paraformaldehyde (PFA)	ChemCruz	Cat#sc-281692
4X Protein Sample Loading Buffer	LI-COR	Cat#928-40004
Tween 20	Sigma-Aldrich	Cat#P7949-500ML
HEPES	Sigma-Aldrich	Cat#H3375-250G
NaCl	Sigma-Aldrich	Cat#106404
Triton X-100	Sigma-Aldrich	Cat#T9284-100ML
Ethylenediaminetetraacetic acid (EDTA)	Sigma-Aldrich	Cat#EDS-100G
Trypsin/EDTA 0.05%/0.02%	PANBiotech	Cat#P10-023100
Dulbecco's Phosphate Buffered Saline (PBS)	Thermo Fisher	Cat#14190094
Poly-L-Lysine	Sigma-Aldrich	Cat#P6282-5MG
Fetal Bovine Serum	Thermo Fisher	Cat#10270106
0.5% Trypsin-EDTA	Thermo Fisher	Cat#15400054
Blocker Casein in PBS	Thermo Fisher	Cat#37528

(*Continued on next page*)

Continued

REAGENT or RESOURCE	SOURCE	IDENTIFIER
Phire Hot Start II DNA-Polymerase	Thermo Fisher	Cat#F122S
dTTP (10 mM)	Invitrogen	Cat#18255018
dATP (10 mM)	Invitrogen	Cat#18252015
dCTP (10 mM)	Invitrogen	Cat#18253013
dGTP (10 mM)	Invitrogen	Cat#18254011
NEBuilder® HiFi DNA Assembly Master Mix	New England BioLabs	Cat#E2621L
Camostat -mesylat	Sigma-Aldrich	Cat#SML0057-10MG
Aloxistatin (E64d)	Selleckchem	Cat#S7393-5MG
Sodium Pyruvate	Thermo Fisher	Cat# 11360070-100mM
Gibco™ Puromycin-Dihydrochlorid	Thermo Fisher	Cat# A1113803-1mL
Blasticidin	InvivoGen	Cat#ant-bl-05-50mg
TaqMan™ Fast Virus 1-Step Master Mix	Thermo Fisher	Cat#4444430-10mL
Critical commercial assays		
Q5 Site-Directed Mutagenesis Kit	New England BioLabs	Cat#E0554
COVID-19 Spike-ACE2 Binding Assay Kit	RayBiotech	Cat#QHD43416
RNeasy Plus Mini Kit (50)	Qiagen	Cat#74134
QIAamp Viral RNA Mini Kit (50)	Qiagen	Cat#52904
Experimental models: Cell lines		
Human: HEK293T cells	ATCC	CRL-3216; RRID: CVCL_0063
Human: CaCo-2 cells	ATCC	HTB-37; RRID: CVCL_0025
Human: A549 cells	ATCC	CCL-185; RRID: CVCL_0023
Mouse: I1 Hybridoma cells	ATCC	CRL-2700; RRID: CVCL_G654
Monkey: Vero E6	ATCC	ATCC Cat# CRL-1586; RRID: CVCL_0574
Oligonucleotides		
Primers for site-directed mutagenesis of the Hu-1 and BA.2 Spike, see Table S1	This paper	N/A
Primers for deletion of IRES-GFP from pCG-SARS-CoV-2 Spike expression constructs Fw: CCGGATCCTGAGAACTTCAGGGTGAGTTTG	Biomers.net	GFPdel_F
Primers for deletion of IRES-GFP from pCG-SARS-CoV-2 Spike expression constructs Rev: TAGGGGGGGGGGCGGAAT	Biomers.net	GFPdel_R
Primer/Probe for qRT-PCR of Human cathepsin L: TaqMan™ Gene Expression Assay (FAM-MGB) Hs00964650_m1	Thermo Fisher	Cat#4331182
Primer/Probe for qRT-PCR of Human TMPRSS2: TaqMan™ Gene Expression Assay (FAM-MGB) Hs01122322_m1	Thermo Fisher	Cat#4331182
Primer/Probe for qRT-PCR of Human GAPDH: TaqMan™ Gene Expression Assay (VIC-TAMRA)	Thermo Fisher	Cat#4310884E
Synthetic SARS-CoV-2-RNA to use as quantitative standard	Twist Bioscience	Cat#102024
Primer for qRT-PCR of N of SARS-CoV-2: Fw: TAATCAGACAAGGAACTGATTA	Biomers.net	HKU-NF
Primer for qRT-PCR of N of SARS-CoV-2: Rev: CGAAGGTGTGACTTCCATG	Biomers.net	HKU-NR

(*Continued on next page*)

Continued

REAGENT or RESOURCE	SOURCE	IDENTIFIER
Probe for qRT-PCR of N of SARS-CoV-2: 5′-6-carboxyfluorescein (FAM)-GCAAATTGTGCAAT TTGCGG-6-carboxytetramethylrhodamine (TAMRA)-3′	Biomers.net	HKU-NP
Recombinant DNA		
Plasmid: pCG_SARS-CoV-2-Hu-1-Spike C-V5-IRES_eGFP (YP_009724390.1)	This study	N/A
Plasmid: pCG_SARS-CoV-2-BA.1-Spike C-V5-IRES_eGFP	This study	N/A
Plasmid: pCG_SARS-CoV-2-BA.2-Spike C-V5-IRES_eGFP	This study	N/A
Plasmid: pCG_SARS-CoV-2-BA.2.12.1-Spike C-V5-IRES_eGFP	This study	N/A
Plasmid: pCG_SARS-CoV-2-BA.4/5-Spike C-V5-IRES_eGFP	This study	N/A
Plasmid: pCSDest_hTMPRSS2	Addgene	Addgene plasmid # 53887; http://n2t.net/addgene:53887; RRID:Addgene_53887
Plasmid: pcDNA3.1_Cathepsin L	Addgene	Addgene plasmid # 11250; http://n2t.net/addgene:11250; RRID:Addgene_11250
Plasmid: pcDNA3.1_Cathepsin B	Addgene	Addgene plasmid # 11249; http://n2t.net/addgene:11249; RRID:Addgene_11249
Plasmid: pCG_ACE2_IRES_eGFP	This study	N/A
Software and algorithms		
GraphPad Prism Version 9.2	GraphPad Software, Inc.	https://www.graphpad.com RRID: SCR_002798
LI-COR Image Studio Version 5.2	LI-COR	www.licor.com/RRID: SCR_015795
CorelDRAW 2021 (64-Bit)	Corel Corporation	www.coreldraw.com/RRID: SCR_014235
BioTek Gen5 3.04	Agilent Technologies	www.biotek.com/RRID:SCR_017317
Fiji 1.53	National Institutes of Health (NIH)	ImageJ.nih.gov/ij/ RRID: SCR_003070
PyMol Version 2.4	Schrödinger	https://pymol.org/2//RRID:SCR_000305
Other		
Dulbecco's Modified Eagle Medium	Thermo Fisher	Cat#41965039
Roswell Park Memorial Institute Medium 1640	Thermo Fisher	Cat#21875034
MEM Non-essential amino acids	Thermo Fisher	Cat#11140035
Opti-MEM Reduced Serum Media	Thermo Fisher	Cat#31985047
Saccharose	Sigma-Aldrich	Cat#S0389-500G
NuPAGE 4–12% Bis-Tris Gels	Invitrogen	Cat#NP0323BOX
Immobilon-FL PVDF membrane	Sigma-Aldrich	Cat#IPFL00010
XbaI restriction enzyme	New England BioLabs	Cat#R0145
MluI restriction enzyme	New England BioLabs	Cat#R0198
384-well Clear Flat Bottom Polystyrene TC-treated Microplates	Corning	Cat#3701
Semi dry blot transfer buffer (10X)	Alfa Aesar	Cat#J63664
NuPAGE™ MES SDS Running Buffer	Invitrogen	Cat#NP0002
TransIT®-LT1 Transfection Reagent	MoBiTec	Cat# MIR2306-1mL

RESOURCE AVAILABILITY

Lead contact

Further information and requests for resources and reagents should be directed to and will be fulfilled by the Lead Contact, Frank Kirchhoff (Frank.Kirchhoff@uni-ulm.de)

Materials availability

All unique reagents generated in this study are listed in the key resources table and available from the lead contact.

Data and code availability

- Primary data are available at https://doi.org/10.17632/6wrpwr84p3.1; Link: https://data.mendeley.com/preview/6wrpwr84p3 upon acceptance of the manuscript. In addition, all data reported in this paper will be shared by the lead contact upon request.
- This study did not generate or analyze datasets or codes.
- Any additional information required to reanalyze the data reported in this paper is available from the lead contact upon request.

EXPERIMENTAL MODEL AND SUBJECT DETAILS

Cells

All cells were cultured at 37°C and 5% CO_2 in a humified atmosphere. HEK293T (human embryonic kidney) cells (ATCC: #CRL3216; derived from a femal fetus in 1973) were cultivated in Dulbecco's Modified Eagle Medium (DMEM) supplemented with 10% (v/v) heat-inactivated fetal bovine serum (FBS), 2 mM L-glutamine, 100 μg/mL streptomycin and 100 U/ml penicillin. Caco2 (human epithelial colorectal adenocarcinoma) cells (ATCC: #HTB-37; isolated from colon tissue derived from a 72-year-old, white male) were cultivated in DMEM containing 20% FBS, 2 mM L-glutamine, 100 μg/mL streptomycin and 100 U/ml penicillin. A549 (human lung carcinoma) cells (ATCC: # CCL-185; derived from a type II pneumocyte lung tumor of a white, 58-year-old male in 1972) stably expressing human ACE2 and/or human TMPRSS2 as well as HEK293T cells stably expressing human ACE2 were kindly provided by Markus Hoffmann and Stefan Pöhlmann (DPZ Göttingen, Germany). A549 cells were maintained in DMEM supplemented with 10% FBS, 2 mM L-glutamine, 100 μg/mL streptomycin, 100 U/ml penicillin, 1 mM NEAA supplement (Non-essential amino acids), 1 mM sodium pyruvate and 2 μg/mL puromycin (to maintain selective pressure for ACE2) and/or 4 μg/mL blasticidin (to maintain selective pressure for TMPRSS2). HEK293T -ACE2 cells were cultivated in DMEM supplemented with 10% (v/v) heat-inactivated FBS, 2 mM L-glutamine, 100 μg/mL streptomycin, 100 U/ml penicillin and 1 μg/mL puromycin. HEK293T stably expressing $GFP_{1\text{-}10/11}$ were kindly provided by Olivier Schwartz (Institute Pasteur, CNRS UMR 3569, Paris, France) and are grown in DMEM supplemented with 10% FBS, 100 μg/mL streptomycin, 100 U/ml penicillin and 1 μg/mL puromycin. Mouse I1-Hybridoma cells (ATCC: #CRL2700) were cultured in Roswell Park Memorial Institute (RPMI) 1640 medium supplemented with 10% (v/v) heat-inactivated fetal bovine serum, 2 mM L-glutamine, 100 μg/mL streptomycin and 100 U/ml penicillin. Vero E6 (African green monkey kidney epithelial) cells (ATCC:#CRL-1586) overexpressing ACE2 and TMPRSS2 were cultured in DMEM supplemented with 10% (v/v) heat-inactivated FBS, 2 mM L-glutamine, 100 μg/mL streptomycin, 100 U/ml penicillin, 1 mM sodium pyruvate.Vero E6-ACE2-TMPRSS2 cells were kindly provided by Viviana Simon (Icahn School of Medicine at Mount Sinai, New York, USA). Purchased cell lines were authenticated by the respective vendor and were not validated further in our laboratory. Cell lines obtained and validated by other groups were not further authenticated. All cell lines used in this study were regularly checked for the presence of mycoplasma by PCR.

Sera from vaccinated individuals

Blood samples of ChAdOx1-nCoV-19/BNT162b2 (donor 1: age 28, female; donor 2: age 36, male) and BNT162b2/BNT162b2 (donor 3: age 58, female; donor 4: age 60, male) vaccinated non-convalescent individuals were obtained after the participants information and written consent. Samples were collected 13−30 days after the second vaccination using S-Monovette Serum Gel tubes (Sarstedt). Before use, the serum was heat-treated at 56°C for 30 min. Ulm University Medical Center Employees who were vaccinated twice, had no indication of previous SARS-CoV-2 infection and expressed interest in participating were included the present study. There were no further inclusion/exclusion parameters. Samples were obtained from both males and females but numbers too low to assess potential gender dependent differences. Ethics approval was provided by the Ethic Committee of Ulm University (vote 99/21– FSt/Sta).

Viruses

VSVΔG(GFP)*VSV-G was kindly provided by Prof. Karl-Klaus Conzelmann (Institute of Virology, LMU Munich, Germany). The SARS-CoV-2 variant B.1.1.529 BA.5 (Omicron BA.5), was kindly provided by Prof. Dr. Florian Schmidt and Dr. Bianca Schulte (University of Bonn). The BetaCoV/Netherlands/01/NL/2020 (NL-02-2020) lineage was obtained from the European Virus Archive. The SARS-COV-2 hCoV-19/USA/CO-CDPHE-2102544747/2021, lineage B.1.1.529, BA.2 (Omicron BA.2) was obtained from the BEI database. SARS-CoV-2 strains were propagated on Vero E6 cells overexpressing ACE2 and TMPRSS2. To this end, 70–90% confluent cells in 75 cm^2 cell culture flasks were inoculated with the SARS-CoV-2 isolate (multiplicity of infection (MOI) of 0.03–0.1) in 3.5 mL serum-free medium. The cells were incubated for 2 h at 37°C, before adding 20 mL medium containing 15 mM HEPES. Virus stocks were harvested as soon as strong cytopathic effect (CPE) became apparent. The virus stocks were centrifuged for 5 min at 1,000 g to remove cellular debris, aliquoted, and stored at −80°C until further use. All procedures

and assays involving genuine SARS-CoV-2 were performed in the BSL3 facilities at the University of Ulm in accordance with institutional biosafety committee guidelines.

Expression constructs

pCG expression plasmids encoding for the Spike protein of SARS-CoV-2 isolate Wuhan-Hu-1 (NCBI reference Sequence YP_009724390.1), pCG1_SARS-2-S-Δ18 (BA.1), pCG1_SARS-2-SΔ18 (BA.2), pCG1_SARS-2-SΔ18 (BA.2.12.1) and pCG1_SARS-2-SΔ18 (BA.4/5) were kindly provided by Stefan Pöhlmann (DPZ Göttingen, Germany). The Spike sequence of all constructs was PCR amplified and subcloned into a pCG-IRESeGFP expression construct by Gibson Assembly repairing the C-terminal deletion and introducing the V5 epitope tag. The SARS-CoV-2 S mutant plasmids were generated using Q5 Site-Directed Mutagenesis Kit (NEB #E0554). For the GFP-Split assay, IRESeGFP was deleted from Spike and ACE2 pCG expression constructs using Q5 Site-Directed Mutagenesis Kit. hTMPRSS2 expression plasmid (Addgene #53887) was provided by Roger Reeves (Johns Hopkins University, Baltimore, United States). hCathepsin L (Addgene # 11250) and hCathepsin B (Addgene # 11249) expression plasmids were provided by Hyeryun Choe (Scripps Research Institute, Jupiter, FL, USA). hACE2 was synthesized by Twist bioscience, PCR amplified, and subcloned into a pCG-IRES_eGFP expression construct using the restriction enzymes XbaI+MluI. All constructs were verified by sequence analysis using a commercial sequencing service (Eurofins Genomics).

METHOD DETAILS

Molecular images

Molecular visualization, analyses and images were performed using the PyMol software (https://pymol.org/2/). Structures of SARS-CoV-2 spike glycoproteins and therapeutic antibodies complexed with Spike RBD were obtained from the Protein DataBank (PDB): BA.2 spike structure alone (PDB ID: 7XIW), BA.2 spike structure bound to human ACE2 (PDB ID: 7XO7) and BA.4/5 spike RBD structure bound to human ACE2 (PDB ID: 7XWA), Bebtelovimab-Spike RBD (PDB ID: 7MMO), Bamlanivimab-Spike RBD (PDB ID: 7KMG), Imdevimab-Spike RBD and Casivirimab-Spike RBD (PDB ID: 6XDG).

Analysis of sequences over time

Proportion of SARS-CoV-2 Spike sequences containing individual amino acid changes compared to the total number of sequences over the time was obtained from covSpectrum by analysis of single variant.

Pseudoparticle Production

To produce pseudotyped VSVΔG(GFP) particles, HEK293T cells were transfected with SARS-CoV-2 spike-expressing vectors using polyethyleneimine (PEI 1 mg/mL in H_2O). 24 h post-transfection, the cells were infected with VSVΔG(GFP) particles pseudotyped with VSV-G at a MOI of 3. Pseudotyped VSVΔG(GFP) particles were harvested 16 h post-infection. Cell debris were removed by centrifugation (500 × g for 5 min). Residual particles carrying VSV-G were blocked by adding 10% (v/v) of I1-Hybridoma supernatant (I1, mouse hybridoma supernatant from CRL-2700; ATCC) to the cell culture supernatant.

Pseudovirus infection

Caco2, A549-ACE2, A549-ACE2-TMPRSS2 cells were infected with 25 μL of VSVΔG(GFP) pseudo particles in 384 well format. HEK293T - ACE2 cells were transfected with TMPRSS2, cathepsin L or cathepsin B expression constructs and, after 24 h, infected with 10 μL of VSVΔG(GFP) pseudo particles in 96 well format. GFP-positive cells were automatically counted using a Cytation 3 microplate reader (BioTek Instruments).

Pseudoparticle inhibition

Caco2 cells were infected in 96 well format with 50 μL of VSVΔG(GFP) pseudo particles, which were preincubated for 30 min at RT with the indicated amounts of monoclonal antibodies (Bamlanivimab (LY-CoV555), Imdevimab (REGN10897), Casivirimab (REGN10933), Bebtelovimab (LY-CoV1404)) or sera from ChAdOx1-nCoV-19/BNT162b2 or BNT162b2/BNT162b2 vaccinated individuals. To assess role of TMPRSS2 and cathepsins for pseudovirus infectivity, Caco2 and A549-ACE2-TMPRSS2 cells were treated with 20 μL of serial dilutions of camostat or E64d for 1 h at 37°C, followed by transduction with 100 μL of VSVΔG(GFP) pseudo particles. Twenty-four hours after infection, GFP-positive cells were automatically counted by a Cytation 3 microplate reader (BioTek Instruments).

Virus treatment

A549-ACE2-TMPRSS2 and Caco2 cells were seeded in 24-wells and incubated with 20 μM of camostat or E64d for 1 h at 37°C before SARS-CoV-2 infection (MOI = 0.05). Sixty microliters of the inoculum were used to infect the cells. Four hours later, input virus was removed and cells were washed with PBS and supplemented with fresh medium. 48 h post-infection supernatants were harvested for qRT-PCR analysis.

qRT-PCR of supernatants

N (nucleoprotein) RNA levels were determined in supernatants collected from SARS-CoV-2-infected cells 48 h post-infection. Total RNA was isolated using the viral RNA minikit according to the manufacturer's instructions. RT-qPCR was performed as previously described using

TaqMan Fast Virus 1-Step master mix and a OneStepPlus real-time PCR system (96-well format, fast mode). Primers were purchased from Biomers and dissolved in RNase-free water. Synthetic SARS-CoV-2-RNA was used as a quantitative standard to obtain viral copy numbers. All reactions were run in duplicates.

qRT-PCR of cells

TMPRSS2 and cathepsin L RNA levels were determined in cells and normalized to GAPDH expression levels. Total RNA was isolated using the RNeasy Plus Mini kit (Qiagen) according to the manufacturer's instructions. qRT-PCR was performed according to the manufacturer's instructions using TaqMan Fast Virus 1-Step Master Mix (Thermo Fisher) and an OneStepPlus Real-Time PCR System (96-well format, fast mode). Primers were purchased from Biomers and dissolved in RNAse free water. All reactions were run in duplicates using TaqMan primers/probes.

Whole-cell and cell-free lysates

For whole-cell lysates preparation, cells were collected and washed in phosphate-buffered Saline (PBS), pelleted and lysed in transmembrane lysis buffer, supplemented with protease inhibitor (1:500). After 5 min of incubation on ice, samples were centrifuged (4°C, 20 min, 20,817 × g) to remove cell debris. Supernatants were transferred to new tubes and mixed with 4x Protein Sample Loading Buffer (LI-COR) containing 10% β-mercaptoethanol, heated at 95°C for 20 min. To prepare the lysates of viral particles, the supernatants were layered on a cushion of 20% sucrose and centrifuged (4°C, 90 min, 20,817 × g). The virus pellet was lysed in transmembrane lysis buffer, already mixed with 4x Protein Sample Loading Buffer (LI-COR) containing 10% β-mercaptoethanol and denaturized at 95°C for 10 min.

SDS-PAGE and immunoblotting

Whole-cell and viral particles lysates were separated on NuPAGE 4–12% Bis-Tris Gels (Invitrogen) for 90 min at 120 V and blotted at constant 30 V for 30 min onto Immobilon-FL PVDF membrane. After the transfer, the membrane was blocked in 1% Casein in PBS. Proteins were stained using primary antibodies directed against rabbit anti-V5 (Cell Signaling #13202; 1:1000), VSV-M (Absolute Antibody, 23H12, #Ab01404–2.0; 1:2000), actin (Anti-beta Actin antibody Abcam, ab8226, 1:5000) and Infrared Dye labeled secondary antibodies (LI-COR IRDye) IRDye 800CW Goat anti-Mouse #926–32210, IRDye 680CW Goat anti-Rabbit (#925–68071), all 1:20,000. Proteins were detected using an LI-COR Odyssey scanner and band intensities were quantified using LI-COR Image Studio version 5.

ACE2 interaction assay

HEK293T cells expressing Spike were collected 48 h after transfection, washed with PBS and divided for simultaneous immunoblotting and ACE2 interaction assay. Cells were lysed in a non-denaturizing transmembrane lysis buffer supplemented with protease inhibitor (1:500) and cell debris pelleted by centrifugation (4°C, 90 min, 20,817 × g). 10 µL of whole-cell lysates were diluted 1:5 in 1x assay diluent buffer (RayBio), added to ACE2 coated wells from the commercial Spike-ACE2 binding assay kit (COVID-19 Spike-ACE2 binding assay II, Ray Bio) and incubated for 2 h with shaking. After washing extensively with the provided wash buffer (RayBio, #EL-ITEMB), the wells were incubated 1 h with 100 µL anti-V5(Mouse) (1:1,000, Cell Signaling, #80076), washed and incubated for 1 h with 100 µL anti-mouse-HRP (1:1,000, RayBio). After washing, the samples were incubated with 50 µL of TMB Substrate Solution (RayBio, #EL-TMB) for 30 min. The reaction was stopped by the addition of 50 µL Stop Solution (RayBio, #ELSTOP) and absorbance was measured at 450 nm with a baseline correction at 650 nm.

GFP-split fusion assay

To detect syncytia formation, HEK293T cells stably expressing GFP_{1-10} or GFP_{11} were mixed 1:1 and seeded at the final density of $8x10^5$ cells/well in 24 well plates pre-coated with poly-L-lysine. Cells were then co-transfected with 350 ng of hACE2 and Spike expressing constructs using LT1. 40 h post-transfection, cells were fixed with 4% PFA and cell nuclei were stained using DAPI. Fluorescence microscopy images were acquired automatically with the Cytation 3 microplate reader (BioTek Instruments) using the DAPI signal for autofocusing. The GFP area was quantified using Fiji ImageJ.

QUANTIFICATION AND STATISTICAL ANALYSIS

Statistical analysis

Viral pseudo-particle infection is presented as the mean of four biological replicates, each consisting of two technical replicates. Infection was normalized to the SARS-CoV-2 Spike Wuhan-1 (Hu-1) or BA.2 sample respectively for the Wuhan-based and BA-2 based mutants. Immunoblot analysis was performed in biological triplicates with one representative blot shown. Band intensity is represented by mean values of three biological replicates. Linear correlations and statistics were performed using GraphPad PRISM 9.2 simple linear regression. Quantification of syncytia formation is presented as the mean of 7 biological replicates, of which one representative image is shown. Interaction between Spike and ACE2 is presented as the mean of four biological replicates, each consisting of two technical replicates. Binding was normalized to the value obtained for the SARS-CoV-2 Spike Wuhan-1 (Hu-1) or BA.2 sample respectively for the Wuhan-based and BA-2 based mutants. Neutralization by sera is presented as the neutralization efficiency by sera derived from four individual donors each performed in two technical replicates. Neutralization by therapeutic antibodies is presented as mean from three biological replicates, each consisting of three technical replicates. $TCID_{50}$ values of serum neutralization and IC50 values of monoclonal antibody inhibition were calculated by a non-linear regression

model with variable slope. Viral N RNA levels obtained from SARS-CoV-2 infected cells are presented as the mean of four biological replicates, each consisting of two technical replicates. Infection was normalized to the untreated cells.

Statistical analyses were performed using GraphPad PRISM 9.2 (GraphPad Software). Statistical significance was analyzed by one-way or two-way ANOVA with multiple comparison against the Wuhan-Hu-1 or BA.2 values. Statistical parameters are specified in the figure legends. No methods were used to determine whether the data met assumptions of the statistical approach. Significant differences are indicated as *$p < 0.05$; **$p < 0.01$; ***$p < 0.001$.